Magnetic moments of decuplet baryons in isospin asymmetric magnetized strange matter

Hrishika P,[*] Manpreet Kaur,[†] Suneel Dutt,[‡] Harleen Dahiya,[§] and Arvind Kumar[‖]
Department of Physics, Dr. B R Ambedkar National Institute of Technology Jalandhar, Jalandhar 144008, Punjab, India

(Received 26 June 2026; revised 10 October 2026; accepted 22 October 2026; published 13 November 2026)

We investigate the in-medium masses and magnetic moments of decuplet baryons $(\Delta, \Sigma^*, \Xi^*, \Omega^-)$ in isospin asymmetric magnetized strange matter at finite temperature within a unified chiral effective framework. Medium modifications of baryons are implemented using the chiral SU(3) quark mean-field (CQMF) model, where constituent quarks interact via scalar (σ, ζ, δ) and vector (ω, ρ, ϕ) meson fields considering the Dirac sea effects. The external magnetic field is incorporated through Landau quantization of charged particles together with anomalous magnetic moments of baryons. The resulting in-medium mass of constituent quarks and decuplet baryons obtained from the CQMF model are subsequently employed as inputs to the chiral constituent quark model (χCQM) to evaluate magnetic moments of baryons. Our results provide a systematic understanding of how dense, hot, and magnetized environments influence the magnetic properties of decuplet baryons.

DOI: 10.1103/5nbm-pc3w

I. INTRODUCTION

The study of hadronic matter under extreme conditions of temperature, density, and magnetic field has become an essential direction in modern nuclear and particle physics. These studies offer a more profound insight into the nonperturbative elements of quantum chromodynamics (QCD), which governs the behavior of quarks and gluons. It has been estimated that strong magnetic fields of the order of $eB \sim 2m_\pi^2$ can be generated at the Relativistic Heavy Ion Collider (RHIC), Brookhaven National Laboratory, and a magnetic field as large as $eB \sim 15m_\pi^2$ is produced at the Large Hadron Collider (LHC) at CERN in noncentral heavy-ion collisions [1–9]. These fields can significantly alter the internal structure and effective properties of hadrons by inducing anisotropy and modifying the QCD vacuum [1,2,10,11].

An intense magnetic field induces many physical phenomena such as chiral magnetic effect [12–14], the chiral magnetic wave [13,15], magnetic catalysis (MC) [16,17], inverse magnetic catalysis (IMC) [18], the directed flow v_1 of D^0 mesons, and the splitting of the spin polarization of the $\Lambda/\bar{\Lambda}$ hyperons [15,19,20]. These phenomena have attracted considerable attention and have been extensively investigated through both theoretical and experimental studies [21,22]. The phenomena of MC and IMC directly modify the chiral condensates, leading to significant changes in hadron masses and their interactions [23–25]. Furthermore, the observable changes in electromagnetic quantities such as quark anomalous magnetic moments, electric dipole moments, and spectral functions [26–31] influence the overall magnetic properties of composite hadrons. Here, the anomalous magnetic moment of quarks refers the dynamically generated magnetic moment [26]. Over the past years, several theoretical frameworks have been developed to study hadronic properties in magnetized environments. These include relativistic mean-field theories [32–34], Nambu–Jona–Lasinio (NJL) frameworks [35,36], their polyakov extended versions (PNJL) [37], QCD sum rules (QCDSR) [38], confined isospin density dependent model [39–41], etc. In these approaches, the inclusion of Dirac sea contributions has been shown to significantly influence the properties of magnetized matter by modifying scalar densities and vacuum structure [42–46].

Magnetic moments and electromagnetic form factors of baryons are the primary observables that gives information about their internal quark structure [47–49]. Magnetic moments of baryons have been investigated through different theoretical models, such as quark meson coupling (QMC) and modified QMC models [50,51], chiral perturbation theory (χPT) [52,53], lattice quantum chromodynamics (LQCD) [54], the chiral SU(3) quark mean-field (CQMF)

[*]Contact author: hrishikap2003@gmail.com
[†]Contact author: ranapreeti803@gmail.com
[‡]Contact author: dutts@nitj.ac.in
[§]Contact author: dahiyah@nitj.ac.in
[‖]Contact author: kumara@nitj.ac.in

Published by the American Physical Society under the terms of the Creative Commons Attribution 4.0 International license. Further distribution of this work must maintain attribution to the author(s) and the published article's title, journal citation, and DOI. Funded by SCOAP³.

model for isospin symmetric nuclear and strange matter, and asymmetric nuclear matter [55–58]. Other approaches including the chiral constituent quark model (χCQM) [59,60] and statistical model [61] have also been employed to investigate baryon magnetic moments. In astrophysical systems, the anomalous magnetic moment of the neutron in dense magnetized matter has been investigated using the variational approach [62], and the influence of medium modified baryonic magnetic moments on neutron star properties in strong magnetic fields has been explored in Ref. [63]. Most recently, heavy baryon chiral perturbation theory (HBχPT) and covariant quark-diquark approaches have provided valuable frameworks for probing baryon structure beyond masses and magnetic moments. This has facilitated investigations of electromagnetic polarizabilities and gravitational form factors, giving essential information about the dynamical and mechanical properties of hadrons [64,65].

The study of magnetic moments of decuplet baryons provides a sensitive probe of chiral symmetry breaking, and medium-induced modifications as these $J^P = \frac{3}{2}^+$ states receive contributions from valence quarks, polarized sea quarks, and orbital angular momentum of the quark sea [66–68]. The internal structures of Δ and other members of the decuplet baryons have been theoretically explored in Refs. [69–71]. However, owing to the very short lifetimes of decuplet baryons, experimental information on their magnetic moments is limited, except for the Ω^- baryon, whose magnetic moment has been measured with reasonable precision. At present, limited experimental data exist primarily for the magnetic moments of the Δ and Ω^- baryons [72–75], with Δ baryons measured with large uncertainties. Within the various frameworks discussed above, the magnetic moments of decuplet baryons are explored in Refs. [50,52–54,57,60,76–80]. These studies have been carried out in both free space and nuclear matter. More recently, the magnetic moments of decuplet baryons have been investigated within the CQMF framework in asymmetric strange hadronic matter at zero magnetic field, demonstrating the sensitivity of the decuplet baryons to the baryon density, isospin asymmetry, and strangeness fraction [81]. The effects of strong magnetic fields on decuplet baryon magnetic moments have also been explored in isospin asymmetric magnetized nuclear matter, highlighting the significant role of the magnetic field in modifying the internal structure and electromagnetic properties of decuplet baryons [82].

Most existing studies are restricted to either nuclear matter or isospin symmetric strange matter, and a comprehensive analysis of decuplet baryon magnetic moment in isospin asymmetric strange matter under the influence of an external magnetic field including the contribution of Dirac sea to scalar densities is still lacking. This motivates the present work where medium effects are incorporated through the CQMF model, wherein quarks are treated as fundamental degrees of freedom and they interact via the exchange of scalar fields (σ, ζ, δ), dilaton field (χ) and vector fields (ω, ρ, ϕ). The external magnetic field is incorporated through Landau quantization of charged particles and anomalous magnetic moments of baryons, which collectively lead to further medium modifications of constituent quarks and baryons. Using the consistently determined in-medium quark and baryon masses from the CQMF model, the magnetic moments of decuplet baryons are subsequently evaluated within the χCQM. In this framework, the valence quarks, the spin polarization of sea quarks, and the orbital angular momentum of the quark sea contribute to the total magnetic moment of decuplet baryons. The presence of strange quarks introduces additional degrees of freedom that significantly influence the properties of hadrons in dense medium. Therefore, this study provides a unified description of decuplet baryon magnetic moments in isospin asymmetric magnetized strange matter by combining chiral mean field model with the chiral constituent quark model.

The structure of the paper is as follows: Section II introduces the chiral SU(3) quark mean-field model with a magnetic field, detailing the associated field equations and density formulas. Section III focuses on the magnetic moments of decuplet baryons within a medium. Section IV presents and discusses the numerical findings, while Sec. V concludes with a summary of the key results of this study.

II. CHIRAL SU(3) QUARK MEAN FIELD (CQMF) MODEL

In the present study, medium-induced modifications of decuplet baryon are investigated using the CQMF framework, where the constituent quarks are confined inside baryons through an effective confining potential [83,84]. We investigate the effective masses and magentic moments of decuplet baryons in the strange medium consisting of nucleons and hyperons. The in-medium masses of constituent quarks arise from their interactions with scalar isoscalar nonstrange σ, and strange ζ, and the scalar isovector δ mesons within the medium. The trace anomaly is incorporated through the dilaton field, χ. The effective Lagrangian density in this model is written as [84,85]

$$\mathcal{L}_{\rm eff} = \mathcal{L}_{\rm chiral} + \mathcal{L}_{\rm mag}, \tag{1}$$

where $\mathcal{L}_{\rm chiral}$ is given by

$$\mathcal{L}_{\rm chiral} = \mathcal{L}_{\rm q0} + \mathcal{L}_{\rm qm} + \mathcal{L}_{\rm VV} + \mathcal{L}_{\Sigma\Sigma} + \mathcal{L}_{\chi \rm SB} + \mathcal{L}_{\Delta m} + \mathcal{L}_{\rm c}. \tag{2}$$

Here, $\mathcal{L}_{\rm q0} = \bar{q} i \gamma^\mu \partial_\mu q$ represents the kinetic contribution of the massless quarks, while $\mathcal{L}_{\rm qm}$ denotes the invariant quark-meson interaction sector [55,86]. $\mathcal{L}_{\Sigma\Sigma}$ and $\mathcal{L}_{VV}$ are the chiral invariant scalar and vector meson self-interaction

terms, respectively. Explicit chiral symmetry breaking is incorporated through $\mathcal{L}_{\chi\mathrm{SB}}$, and the explicit strange quark mass contribution is introduced through $\mathcal{L}_{\Delta m}$. The last term, $\mathcal{L}_c$, represents the confinement of constituent quarks inside the baryons. The second term in Eq. (1), $\mathcal{L}_{\mathrm{mag}}$, is added in order to include the external magnetic field effects. It describes the coupling of baryons to the external magnetic field, including the effects of anomalous magnetic moments (AMM) [32,87–89] and is given by

$$\mathcal{L}_{\mathrm{mag}} = -\bar{\psi}_i q_i \gamma_\mu A^\mu \psi_i - \frac{1}{2}\kappa_i \bar{\psi}_i \sigma^{\mu\nu} F_{\mu\nu} \psi_i - \frac{1}{4} F^{\mu\nu} F_{\mu\nu}. \tag{3}$$

In the above equation, $\bar{\psi}_i$ and q_i denote the wave function and electric charge associated with the i^{th} baryon, respectively. The second term represents the tensorial interaction with the electromagnetic field, where $F_{\mu\nu} = \partial_\mu A_\nu - \partial_\nu A_\mu$, and $\sigma^{\mu\nu} = \frac{i}{2}[\gamma^\mu, \gamma^\nu]$. The quantity, κ_i denotes the AMM of the baryon in terms of nuclear magneton μ_N. The inclusion of the electromagnetic interaction modifies the single particle energy spectrum, and using these modified energy eigenvalues, the thermodynamic potential can be modified as

$$\Omega = \Omega_{\mathrm{DS}} + \Omega_{\mathrm{med}} - \mathcal{L}', \tag{4}$$

where Ω_{DS} and Ω_{med} denote the contributions of the Dirac sea (DS) and the Fermi sea of baryons, respectively, to the total thermodynamic potential, and the last term $\mathcal{L}'$ is defined as $\mathcal{L}' = \mathcal{L}_{VV} + \mathcal{L}_{\Sigma\Sigma} + \mathcal{L}_{\chi\mathrm{SB}}$. For spin-$\frac{1}{2}$ charged baryons ($i = p, \Sigma^\pm, \Xi^-$), the contributions from the Dirac sea to the thermodynamic potential are written as [43,45,46]

$$\sum_i \Omega_{\mathrm{DS}}^{\mathrm{charged},i} = -\sum_i \frac{|q_i|B}{2\pi}\left[\left\{\sum_{\bar{\nu}=0}^{\bar{\nu}_{\max}^{(s=1)}} \int_{-\infty}^{\infty} \frac{dk_z}{2\pi}\epsilon^i_{k,\bar{\nu},s}\right\} + \left\{\sum_{\bar{\nu}=1}^{\bar{\nu}_{\max}^{(s=-1)}} \int_{-\infty}^{\infty} \frac{dk_z}{2\pi}\epsilon^i_{k,\bar{\nu},s}\right\}\right]. \tag{5}$$

Here, we can see that the continuous transverse momentum integration is replaced by a discrete sum over Landau levels $\bar{\nu} = 0, 1, 2, \ldots \bar{\nu}_{\max}$, due to the quantization of charged particle orbits in the external magnetic field [90]. For neutral baryons ($i = n, \Lambda, \Sigma^0, \Xi^0$), which do not undergo Landau quantization, the potential takes the form

$$\sum_i \Omega_{\mathrm{DS}}^{\mathrm{neutral},i} = -\sum_i \sum_{s=\pm1} \int \frac{d^3k}{(2\pi)^3}\epsilon^i_{k,s}. \tag{6}$$

The medium contribution to thermodynamic potential for charged baryons is given by

$$\sum_i \Omega_{\mathrm{med}}^{\mathrm{charged},i} = -T\sum_i \frac{|q_i|B}{2\pi}\left[\sum_{\bar{\nu}=0}^{\bar{\nu}_{\max}^{(s=1)}} \int_{-\infty}^{\infty} \frac{dk_z}{2\pi}\{\ln(1+e^{-\beta(\epsilon^i_{k,\bar{\nu},s}-\nu_i^*)}) + \ln(1+e^{-\beta(\epsilon^i_{k,\bar{\nu},s}+\nu_i^*)})\} + \sum_{\bar{\nu}=1}^{\bar{\nu}_{\max}^{(s=-1)}} \int_{-\infty}^{\infty} \frac{dk_z}{2\pi}\{\ln(1+e^{-\beta(\epsilon^i_{k,\bar{\nu},s}-\nu_i^*)}) + \ln(1+e^{-\beta(\epsilon^i_{k,\bar{\nu},s}+\nu_i^*)})\}\right], \tag{7}$$

and for neutral baryons, the contribution is given as

$$\sum_i \Omega_{\mathrm{med}}^{\mathrm{neutral},i} = -T\sum_i \sum_{s=\pm1} \int \frac{d^3k}{(2\pi)^3}[\ln(1+e^{-\beta(\epsilon^i_{k,s}-\nu_i^*)}) + \ln(1+e^{-\beta(\epsilon^i_{k,s}+\nu_i^*)})], \tag{8}$$

where β is the inverse of temperature T. The parameter $s = \pm 1$ represents the spin up and spin down projections, and ν_i^* is the effective chemical potential of baryons, which is a function of vector fields ω, ρ and ϕ. In Eqs. (5) and (7), $\epsilon^i_{k,\bar{\nu},s}$ denotes the single particle energy spectra of the ith charged baryon whereas $\epsilon^i_{k,s}$ in Eqs. (6) and (8) denotes the energy spectra of the ith neutral baryon in the presence of a magnetic field and are given as

$$\epsilon^i_{k,\bar{\nu},s} = \sqrt{k_z^2 + \left(\sqrt{2\bar{\nu}|q_i|B + \mathcal{M}_i^{*2}} - s\kappa_i B\right)^2}, \tag{9}$$

and

$$\epsilon^i_{k,s} = \sqrt{k_z^2 + \left(\sqrt{k_x^2 + k_y^2 + \mathcal{M}_i^{*2}} - s\kappa_i B\right)^2}. \tag{10}$$

In Eqs. (9) and (10), the components k_x and k_y represent the transverse momentum of the baryon, while k_z denotes the longitudinal momentum component relative to the direction of the external magnetic field. Also, $\mathcal{M}_i^*$ is the in-medium mass of the ith baryon defined as

TABLE I. Various parameters and coupling constants utilized in the present calculations [100].

k_0	4.94	k_1	2.12	k_2	−10.16
k_3	−5.38	k_4	−0.06	g_4	37.5
d	0.182	ρ_0 (fm^{-3})	0.16	m_v (MeV)	673.648
f_π (MeV)	93	f_K (MeV)	115	m_π (MeV)	139
m_K (MeV)	496	m_ω (MeV)	783	m_ϕ (MeV)	1020
σ_0 (MeV)	−93	ζ_0 (MeV)	−96.87	χ_0 (MeV)	254.38
$g_\sigma^{u,d}$	2.72	g_σ^s	0	$g_\zeta^{u,d}$	0
g_ζ^s	3.847	$g_\delta^{u,d}$	2.72	g_δ^s	0
$g_\omega^{u,d}$	3.23	g_ω^s	0	$g_\rho^{u,d}$	3.23
g_ρ^s	0	$g_\phi^{u,d}$	0	g_ϕ^s	4.57
a	0.12	$a\alpha^2 = a\beta^2$	0.0243	$a\zeta^2$	0.0053
$a\gamma^2$	0.0014	M_η (MeV)	547.862	$M_{\eta'}$ (MeV)	957.78
M_{η_c} (MeV)	2983.5	M_D (MeV)	1869	M_{D_s} (MeV)	1968
m_c (MeV)	1270	...	...	...	...

$$\mathcal{M}_i^* = \sqrt{E_i^{*2} - \langle p_{i,\mathrm{cm}}^2 \rangle}, \tag{11}$$

where E_i^* denotes the effective in-medium energy of the baryon, and $\langle p_{i,\mathrm{cm}}^2 \rangle$ represents the correction arising from the spurious center of mass motion of the constituent quarks and is evaluated as the sum of the average squared momenta of the individual constituent quarks [91,92],

$$\langle p_{i,\mathrm{cm}}^2 \rangle = \sum_q \langle p_{\mathrm{cm}}^{*2} \rangle_q = \sum_q \frac{11 e_q^* + m_q^*}{6(3e_q^* + m_q^*)} (e_q^{*2} - m_q^{*2}). \tag{12}$$

Here, e_q^* is the effective energy of constituent quarks, and m_q^* is the effective quark mass, which is given by

$$m_q^* = -g_\sigma^q \sigma - g_\zeta^q \zeta - g_\delta^q I^{3q} \delta + m_{q0}, \tag{13}$$

where the g_σ^q, g_ζ^q, and g_δ^q are the coupling strength of quarks with the σ, ζ, and δ fields, and m_{q0} is the bare quark mass contribution which is zero for nonstrange quarks and finite for strange quarks. The vacuum masses of constituent quarks are expressed in terms of vacuum values of fields, σ_0 and ζ_0 as $m_u = m_d = -\frac{g_s}{\sqrt{2}}\sigma_0 = -g_\sigma^q \sigma_0$ and $m_s = -g_\zeta^s \zeta_0 + m_{q0}$. The numerical values of the coupling constants and vacuum fields are listed in Tables I and II. The medium-induced modifications of the constituent quark masses lead to corresponding changes in the effective energies of the quarks, which are reflected in the effective energies of the baryons. Thus, the effective energy of the ith baryon can be expressed in terms of the effective energies of its constituent quarks as

$$E_i^* = \sum_q n_{qi} e_q^* + E_{i,\mathrm{spin}}, \tag{14}$$

where n_{qi} denotes the number of q quarks in the ith baryon. The term $E_{i,\mathrm{spin}}$ accounts for the spin-spin interaction among the constituent quarks and serves as a correction to the baryon energy. The isospin asymmetry parameter is defined as $I_a = -\sum_i \frac{I^{3i}\rho_v^i}{\rho_B}$, where I^{3i} represents the third component of isospin, and ρ_B is the total baryonic density of the medium. The strangeness fraction is given by $f_s = \sum_i \frac{|s_i|\rho_v^i}{\rho_B}$, where $|s_i|$ represents the number of strange quarks in the ith baryon. To determine the equilibrium state of the system for given values of ρ_B, I_a, f_s, T, and magnetic field eB, the total thermodynamic potential is minimized with respect to the mesonic fields $(\sigma, \zeta, \delta, \chi, \omega, \rho, \phi)$ [93–95] such that

$$\frac{\partial\Omega}{\partial\sigma} = \frac{\partial\Omega}{\partial\zeta} = \frac{\partial\Omega}{\partial\delta} = \frac{\partial\Omega}{\partial\chi} = \frac{\partial\Omega}{\partial\omega} = \frac{\partial\Omega}{\partial\rho} = \frac{\partial\Omega}{\partial\phi} = 0. \tag{15}$$

TABLE II. Baryon-meson coupling constants used in the present calculation.

$g_{\sigma p}$	6.64	$g_{\omega p}$	9.69
$g_{\zeta p}$	0	$g_{\rho p}$	8.89
$g_{\delta p}$	2.72	$g_{\phi p}$	0
$g_{\sigma n}$	6.64	$g_{\omega n}$	9.69
$g_{\zeta n}$	0	$g_{\rho n}$	8.89
$g_{\delta n}$	2.72	$g_{\phi n}$	0
$g_{\sigma\Lambda}$	5.44	$g_{\omega\Lambda}$	8.85
$g_{\zeta\Lambda}$	3.85	$g_{\rho\Lambda}$	0
$g_{\delta\Lambda}$	0	$g_{\phi\Lambda}$	−4.57
$g_{\sigma\Sigma}$	5.44	$g_{\omega\Sigma}$	12.28
$g_{\zeta\Sigma}$	3.85	$g_{\rho\Sigma}$	12.28
$g_{\delta\Sigma}$	2.72	$g_{\phi\Sigma}$	−4.57
$g_{\sigma\Xi}$	2.72	$g_{\omega\Xi}$	7.27
$g_{\zeta\Xi}$	7.69	$g_{\rho\Xi}$	3.23
$g_{\delta\Xi}$	2.72	$g_{\phi\Xi}$	−9.14

The minimization conditions lead to the following nonlinear coupled mean-field equations:

$$\frac{\partial\Omega}{\partial\sigma} = k_0\chi^2\sigma - 4k_1(\sigma^2+\zeta^2+\delta^2)\sigma - 2k_2(\sigma^3+3\sigma\delta^2) - 2k_3\chi\sigma\zeta - \frac{d}{3}\chi^4\left(\frac{2\sigma}{\sigma^2-\delta^2}\right) + \left(\frac{\chi}{\chi_0}\right)^2 m_\pi^2 f_\pi - \left(\frac{\chi}{\chi_0}\right)^2 m_\omega\omega^2\frac{\partial m_\omega}{\partial\sigma} - \left(\frac{\chi}{\chi_0}\right)^2 m_\rho\rho^2\frac{\partial m_\rho}{\partial\sigma} - \sum_i g_\sigma^i\rho_s^i = 0, \tag{16}$$

$$\frac{\partial\Omega}{\partial\zeta} = k_0\chi^2\zeta - 4k_1(\sigma^2+\zeta^2+\delta^2)\zeta - 4k_2\zeta^3 - k_3\chi(\sigma^2-\delta^2) - \frac{d}{3}\frac{\chi^4}{\zeta} + \left(\frac{\chi}{\chi_0}\right)^2\left[\sqrt{2}m_K^2 f_K - \frac{1}{\sqrt{2}}m_\pi^2 f_\pi\right] - \left(\frac{\chi}{\chi_0}\right)^2 m_\phi\phi^2\frac{\partial m_\phi}{\partial\zeta} - \sum_i g_\zeta^i\rho_s^i = 0, \tag{17}$$

$$\frac{\partial\Omega}{\partial\delta} = k_0\chi^2\delta - 4k_1(\sigma^2+\zeta^2+\delta^2)\delta - 2k_2(\delta^3+3\sigma^2\delta) + 2k_3\chi\delta\zeta + \frac{2}{3}d\chi^4\left(\frac{\delta}{\sigma^2-\delta^2}\right) - \sum_i g_\delta^i I^{3i}\rho_s^i = 0, \tag{18}$$

$$\frac{\partial\Omega}{\partial\chi} = k_0\chi(\sigma^2+\zeta^2+\delta^2) - k_3(\sigma^2-\delta^2)\zeta + \chi^3\left[1+\ln\left(\frac{\chi^4}{\chi_0^4}\right)\right] + (4k_4-d)\chi^3 - \frac{4}{3}d\chi^3\ln\left(\frac{(\sigma^2-\delta^2)\zeta}{\sigma_0^2\zeta_0}\left(\frac{\chi}{\chi_0}\right)^3\right) + \frac{2\chi}{\chi_0^2}\left[m_\pi^2 f_\pi\sigma + \left(\sqrt{2}m_K^2 f_K - \frac{1}{\sqrt{2}}m_\pi^2 f_\pi\right)\zeta\right] - \frac{\chi}{\chi_0^2}(m_\omega^2\omega^2 + m_\rho^2\rho^2 + m_\phi^2\phi^2) = 0, \tag{19}$$

$$\frac{\partial\Omega}{\partial\omega} = \frac{\chi^2}{\chi_0^2}m_\omega^2\omega + 4g_4\omega^3 + 12g_4\omega\rho^2 - \sum_i g_\omega^i\rho_v^i = 0, \tag{20}$$

$$\frac{\partial\Omega}{\partial\rho} = \frac{\chi^2}{\chi_0^2}m_\rho^2\rho + 4g_4\rho^3 + 12g_4\omega^2\rho - \sum_i g_\rho^i I^{3i}\rho_v^i = 0, \tag{21}$$

$$\frac{\partial\Omega}{\partial\phi} = \frac{\chi^2}{\chi_0^2}m_\phi^2\phi + 8g_4\phi^3 - \sum g_\phi^i\rho_v^i = 0. \tag{22}$$

The number density of the ith baryon, ρ_v^i, is obtained from the medium contribution to the thermodynamic potential. For charged baryons, it is given by

$$\rho_v^i = \frac{|q_i|B}{2\pi^2}\left[\sum_{\bar\nu=0}^{\bar\nu_{\max}^{(s=1)}}\int_0^\infty dk_z\left\{\frac{1}{1+e^{\beta(\epsilon_{k,\bar\nu,s}^i-\nu_i^*)}} - \frac{1}{1+e^{\beta(\epsilon_{k,\bar\nu,s}^i+\nu_i^*)}}\right\} + \sum_{\bar\nu=1}^{\bar\nu_{\max}^{(s=-1)}}\int_0^\infty dk_z\left\{\frac{1}{1+e^{\beta(\epsilon_{k,\bar\nu,s}^i-\nu_i^*)}} - \frac{1}{1+e^{\beta(\epsilon_{k,\bar\nu,s}^i+\nu_i^*)}}\right\}\right]. \tag{23}$$

For neutral baryons, the corresponding expression is given as

$$\rho_v^i = \sum_{s=\pm1}\int\frac{d^3k}{(2\pi)^3}\left[\frac{1}{1+e^{\beta(\epsilon_{k,s}^i-\nu_i^*)}} - \frac{1}{1+e^{\beta(\epsilon_{k,s}^i+\nu_i^*)}}\right]. \tag{24}$$

By neglecting the Dirac sea contribution to the thermodynamic potential, the medium contribution to the scalar density ρ_s^i for charged baryons is given by

$$\rho_{s,\mathrm{med}}^i = \frac{|q_i|B}{2\pi^2}\left[\sum_{\bar\nu=0}^{\bar\nu_{\max}^{(s=1)}}\mathcal{M}_i^*\int_0^\infty dk_z\frac{\sqrt{\mathcal{M}_i^{*2}+2\bar\nu|q_i|B} - s\kappa_i B}{\epsilon_{k,\bar\nu,s}^i\sqrt{\mathcal{M}_i^{*2}+2\bar\nu|q_i|B}}\left\{\frac{1}{1+e^{\beta(\epsilon_{k,\bar\nu,s}^i-\nu_i^*)}} + \frac{1}{1+e^{\beta(\epsilon_{k,\bar\nu,s}^i+\nu_i^*)}}\right\} + \sum_{\bar\nu=1}^{\bar\nu_{\max}^{(s=-1)}}\mathcal{M}_i^*\int_0^\infty dk_z\frac{\sqrt{\mathcal{M}_i^{*2}+2\bar\nu|q_i|B} - s\kappa_i B}{\epsilon_{k,\bar\nu,s}^i\sqrt{\mathcal{M}_i^{*2}+2\bar\nu|q_i|B}}\left\{\frac{1}{1+e^{\beta(\epsilon_{k,\bar\nu,s}^i-\nu_i^*)}} + \frac{1}{1+e^{\beta(\epsilon_{k,\bar\nu,s}^i+\nu_i^*)}}\right\}\right], \tag{25}$$

while for neutral baryons it takes the form

$$\rho^i_{s,\mathrm{med}} = \mathcal{M}^*_i \sum_{s=\pm1} \int \frac{d^3k}{(2\pi)^3} \frac{\sqrt{k_x^2+k_y^2+\mathcal{M}^{*2}_i} - s\kappa_i B}{\epsilon^i_{k,s}\sqrt{k_x^2+k_y^2+\mathcal{M}^{*2}_i}} \times \left[\frac{1}{1+e^{\beta(\epsilon^i_{k,s}-\nu^*_i)}} + \frac{1}{1+e^{\beta(\epsilon^i_{k,s}+\nu^*_i)}}\right]. \quad (26)$$

In this work, the magnetized DS contribution is included within the weak magnetic field approximation. The baryon propagator is expanded in powers of the magnetic field via q_iB and κ_iB, retaining terms up to second order. The self-energy contribution, which diverges without a magnetic field, is disregarded due to its negligible size. The finite magnetic field-dependent contribution modifies the scalar density through vacuum polarization effects induced by the external magnetic field [96]. Consequently, the scalar density receives an additional contribution from the magnetized Dirac sea, which is given by [85,97–99]

$$\rho_s^{\mathrm{DS},i} = -\frac{1}{4\pi^2}\left[\frac{(q_iB)^2}{3\mathcal{M}^*_i} + \{(\kappa_iB)^2\mathcal{M}^*_i + |q_iB|(\kappa_iB)\} \times \left(\frac{1}{2} + 2\ln\left(\frac{\mathcal{M}^*_i}{\mathcal{M}_i}\right)\right)\right]. \quad (27)$$

Note that in the present work we investigate the properties of decuplet baryons in the strange medium consisting of nucleons and hyperons. Therefore, first the coupled systems of equations defined in Eqs. (16) to (22) are solved considering nucleons and hyperons through summation over their scalar and number densities. This gives the in-medium values of scalar and vector fields as well as the effective constituent quark masses.

To calculate the decuplet baryon masses in this strange medium, we proceed as follows. In the presence of an external magnetic field, charged decuplet baryons are affected by both Landau quantization and AMM. Therefore, to incorporate the effects of the external magnetic field, we set the momentum in Eqs. (9) and (10) to zero, and the resulting energy expression defines the effective mass of the spin-$\frac{3}{2}$ charged baryon, which is given by [101]

$$M^*_{i,\bar{\nu},s} = \sqrt{\mathcal{M}^{*2}_i + 2\bar{\nu}|q_i|B} - s\kappa_iB. \quad (28)$$

The lowest Landau level ($\bar{\nu}=0$) is occupied by $s=\{+1,+3\}$ for positively charged decuplet baryons ($i=\Delta^{++}$, Δ^+, and Σ^{*+}), whereas for negatively charged baryons ($i=\Delta^-$, Σ^{*-}, and Ω^-) by $s=\{-3,-1\}$, corresponding to the lowest orbital momentum. For neutral decuplet baryons ($i=\Delta^0$, Σ^{*0}, and Ξ^{*0}), Landau quantization is absent, and the effective mass receives contributions only from the AMM,

$$M^*_{i,s} = \mathcal{M}^*_i - s\kappa_iB, \quad (29)$$

where $s=\pm3,\pm1$. Equations (28) and (29) are used to obtain the in-medium masses of decuplet baryons. The effective mass $\mathcal{M}^*_i$ appearing in these equations is calculated using Eq. (11) which further depends upon in-medium scalar and vector fields through Eq. (14). The scalar and vector fields used in these relations are the ones evaluated in the strange hadronic medium consisting of nucleons and hyperons. Furthermore, while calculating the effective masses of decuplet baryons, $E_{i,\mathrm{spin}}$ is fitted so as to produce the correct vacuum mass of corresponding baryon.

III. MAGNETIC MOMENT OF BARYONS

In this section, the magnetic moments of baryons are evaluated within a framework that combines the CQMF model with the chiral constituent quark model (χCQM), where the masses of baryons are given as an input to calculate their magnetic moment. The χCQM framework incorporates the chiral symmetry breaking effects through quark-Goldstone boson interactions. The total magnetic moment of a baryon is written as the sum of contributions from valence quarks, sea quarks, and the orbital angular momentum of sea quarks as given in Eq. (32). Sea quarks arise due to chiral fluctuations of valence quarks via the emission of Goldstone bosons (GBs),

$$q^{\uparrow(\downarrow)} \to \mathrm{GB}^0 + q'^{\downarrow(\uparrow)} \to (q\bar{q}') + q'^{\downarrow(\uparrow)}, \quad (30)$$

where the emitted GB subsequently splits into a quark-antiquark pair, generating the sea quark content of the baryon [67,78,102–108]. The effective interaction between quarks and the GB is described by the Lagrangian [59],

$$\mathcal{L}_{\mathrm{int}} = g_{15}\bar{q}(\Phi')q, \quad (31)$$

where g_{15} denotes the quark GB coupling strength, and Φ' represents the GB field matrix. The field Φ' incorporates the pseudoscalar mesons arising from the spontaneous breaking of chiral symmetry and is expressed as

$$\Phi' = \begin{pmatrix} \frac{\pi^0}{\sqrt{2}} + \beta\frac{\eta}{\sqrt{6}} + \xi\frac{\eta'}{4\sqrt{3}} - \gamma\frac{\eta_c}{4} & \pi^+ & \alpha K^+ & \gamma\bar{D}^0 \\ \pi^- & -\frac{\pi^0}{\sqrt{2}} + \beta\frac{\eta}{\sqrt{6}} + \xi\frac{\eta'}{4\sqrt{3}} - \gamma\frac{\eta_c}{4} & \alpha K^0 & \gamma D^- \\ \alpha K^- & \alpha\bar{K}^0 & -2\beta\frac{\eta}{\sqrt{6}} + \xi\frac{\eta'}{4\sqrt{3}} - \gamma\frac{\eta_c}{4} & \gamma D_s^- \\ \gamma D^0 & \gamma D^+ & \gamma D_s^+ & -3\xi\frac{\eta'}{4\sqrt{3}} + 3\gamma\frac{\eta_c}{4} \end{pmatrix}$$

The parameters α, β, ξ, and γ encode the effects of SU(3) and SU(4) symmetry breaking associated with the emission of kaons, eta, and charmed mesons, respectively. The contributions of valence, sea quarks, and orbital angular momentum of sea quarks to the total magnetic moment of a baryon are expressed as

$$\mu_B^* = \mu_{\rm val}^* + \mu_{\rm sea}^* + \mu_{\rm orb}^*, \tag{32}$$

where

$$\mu_{\rm val}^* = \sum_{q=u,d,s,c} \Delta q_{\rm val} \mu_q^*, \qquad \mu_{\rm sea}^* = \sum_{q=u,d,s,c} \Delta q_{\rm sea} \mu_q^*,$$
$$\text{and} \quad \mu_{\rm orb}^* = \sum_{q=u,d,s,c} \Delta q_{\rm val} \mu^*(q^+ \to q'^-). \tag{33}$$

Here, $\Delta q_{\rm val}$ and $\Delta q_{\rm sea}$ denote the spin polarizations of the constituent valence and sea quarks, respectively, and are given in Ref. [109]. The term $\mu^*(q^+ \to q'^-)$ denotes the orbital magnetic moment associated with a specific chiral fluctuation process. To incorporate quark confinement effects together with relativistic corrections to the effective quark magnetic moments, the following expressions are employed for the constituent quarks of a given baryon:

$$\mu_u^* = \frac{2M_N}{3m_u^*}\left(1 - \frac{\Delta M}{M_i^*}\right), \qquad \mu_d^* = -\frac{m_u^*}{2m_d^*}\mu_u^*, \tag{34}$$

$$\mu_s^* = \frac{m_d^*}{m_s^*}\mu_d^*, \qquad \mu_c^* = \frac{m_u^*}{m_c}\mu_u^*. \tag{35}$$

Here, M_N is the nucleon mass, and M_i^* is evaluated using Eqs. (28) and (29), taking the lowest value of mass of each decuplet baryon. The term $\Delta M = M_i^* - M_{i,\rm vac}$, where $M_{i,\rm vac}$, represents the vacuum mass of the baryon. In the present calculations, the orbital contributions from the four quark flavors u, d, s, and c are included, and the explicit expressions for the transition magnetic moments are given in Ref. [59].

IV. RESULTS AND DISCUSSION

In this section, we present the results of the medium modified masses and magnetic moments of decuplet baryons in isospin asymmetric magnetized strange matter at finite density ρ_B and temperature T. As can be seen from Eqs. (34) and (35), the value of the magnetic moments of constituent quarks are determined from the effective masses of both quarks and baryons, which themselves are the functions of the scalar fields. Consequently, analyzing the magnetic field dependence of scalar fields and baryon masses is crucial for evaluating the medium modification of magnetic moments of baryons and is presented in coming subsections.

A. In-medium scalar fields in magnetized strange matter

Within the CQMF model, the in-medium mean fields are obtained by solving the coupled equations of motion given in Eqs. (16)–(22). Figure 1 shows the variation of the scalar fields σ, ζ, and δ as functions of the magnetic field eB/m_π^2 for different baryon densities ($\rho_B = 0, \frac{\rho_0}{2}, \rho_0$) and strangeness fractions ($f_s = 0, 0.3, 0.7$), at temperature $T = 100$ MeV. The left and right panels correspond to isospin symmetric matter ($I_a = 0$) and isospin asymmetric matter ($I_a = 0.3$), respectively.

For given isospin asymmetry I_a, all the fields become progressively more negative, across all medium parameters with increase in magnetic field. From Figs. 1(a) and 1(b), we observe that the magnitude of the nonstrange scalar field σ increases with increase in magnetic field within the strange medium. This finite increase as demonstrated in studies in Ref. [85] results from the contribution of the Dirac sea (DS), which shows negligible variation when the contribution of DS is not considered. The solutions of the scalar fields exist only up to a critical magnetic field $eB \sim 5.56m_\pi^2$ in the strange matter at finite densities. From Fig. 1(a), we observe that the variation in the magnitude of the σ field becomes more pronounced beyond $eB = 4m_\pi^2$. At zero baryon density ($\rho_B = 0$), the magnitude of the σ field remains relatively larger, with a value of -94.24 MeV, compared with it's values at finite baryon densities, where it changes to -64.44 and -78.39 MeV at $\rho_B = \frac{\rho_0}{2}$ and ρ_0, respectively, for $f_s = 0.3$ and zero magnetic field. The inclusion of a finite strangeness fraction f_s has a negligible impact on the behavior of the σ field, indicating its weak sensitivity to the strangeness content of the medium. From Fig. 1(b), as we increase the isospin asymmetry from $I_a = 0$ to 0.3, we observe an increase in the magnitude of the σ field. At zero magnetic field and for strangeness fraction $f_s = 0.7$, we observe a small shift of 0.44 (0.27) MeV at $\rho_B = \frac{\rho_0}{2}(\rho_0)$ in the magnitude of σ field.

The strange scalar field ζ also shows an increase in the magnitude with magnetic field which lies in a narrower range compared to σ field as shown in the Figs. 1(c) and 1(d). For example, in Figs. 1(a) and 1(c) for baryonic density $\rho_B = \frac{\rho_0}{2}$, $I_a = 0$, and $f_s = 0.3$, the magnitude of scalar field $\zeta(\sigma)$ is observed to be -92.35 (-78.86) MeV at zero magnetic field, -96.59 (-89.11) MeV at $eB = 3m_\pi^2$. and -113.35 (-127.22) MeV at $eB = 5m_\pi^2$. We observe a small decrease of 0.83% in magnitude of ζ field as f_s is increased from 0.3 to 0.7 at $\rho_B = \rho_0$ and $eB = 5m_\pi^2$, indicating the response of the strange condensate in the medium. As observed for the σ field, the magnitude of the ζ field decreases with increasing baryonic density. For $f_s = 0.7$, the corresponding values of the ζ field at $\rho_B = \frac{\rho_0}{2}$ and ρ_0 are -92.35 (-113.35) MeV and -86.98 (-100.89) MeV at $eB = 0m_\pi^2$ $(5m_\pi^2)$, respectively. With increase in I_a from 0 to 0.3, a negligible rise in magnitude of value 0.007 MeV is

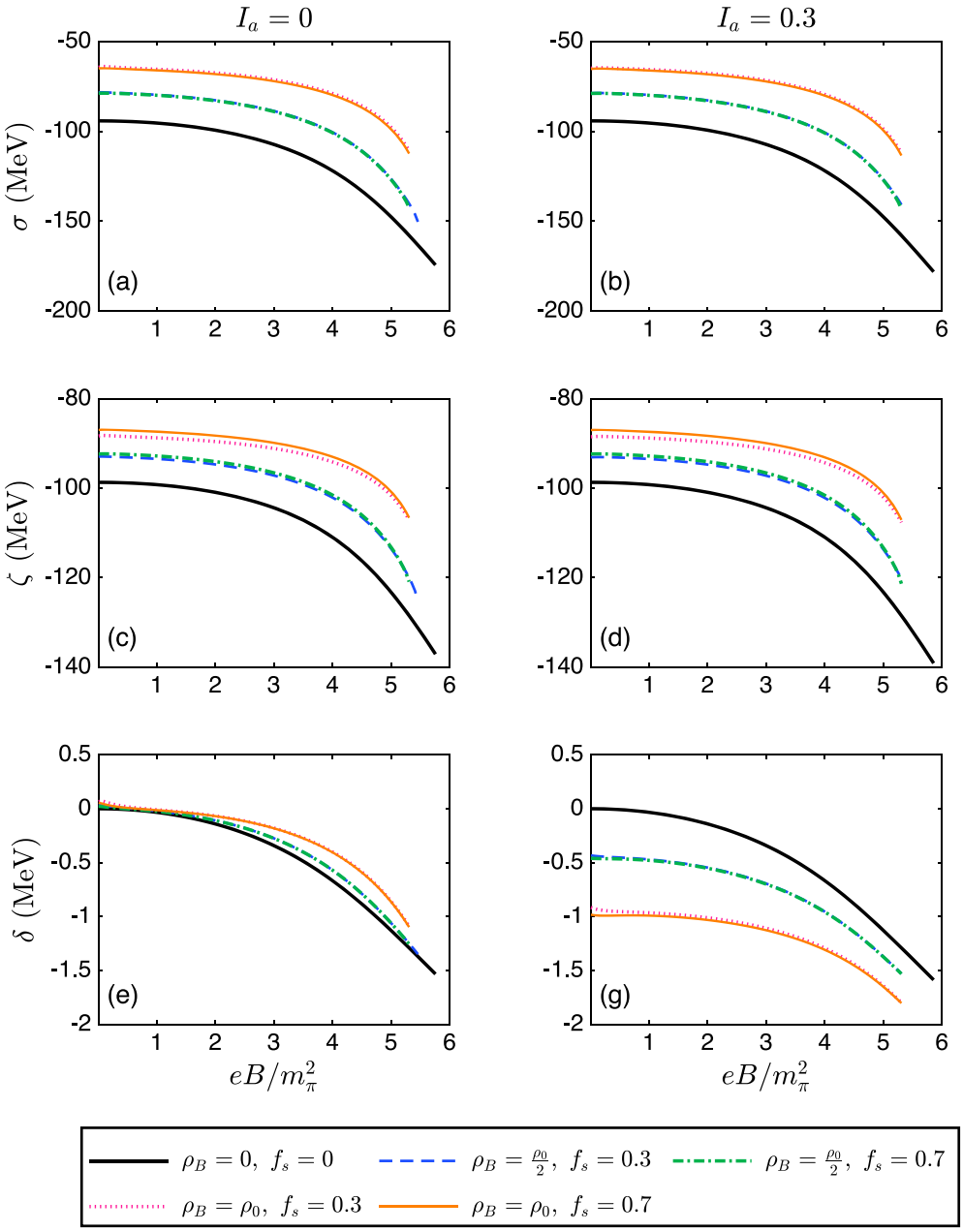


FIG. 1. Variation of scalar fields (σ, ζ, and δ) with magnetic field eB/m_π^2 for isospin symmetric $I_a = 0$ [panels (a), (c), and (e)] and isospin asymmetric $I_a = 0.3$ [panels (b), (d), and (f)] magnetized strange medium at temperature T=100 MeV. Each panel shows the results corresponding to different baryon densities ρ_B and strangeness fraction f_s.

observed, reflecting the ζ field's weak sensitivity to isospin asymmetry.

Figures 1(e) and 1(f) show the variation of scalar-isovector field δ as a function of magnetic field. For isospin symmetric matter $I_a = 0$, the δ field is observed to be nearly zero for the vacuum ($\rho_B = 0$) and finite densities ($\rho_B = \frac{\rho_0}{2}, \rho_0$) cases across all strangeness fractions f_s at zero magnetic field. This is expected because, in the isospin symmetric matter, the number of u and d quarks are equal; therefore, the δ field vanishes. However, as the magnetic field strength is increased, the magnitude of the δ field also increases, showing nearly identical behavior across different baryonic densities and strangeness fractions. Figure 1(f) shows a pronounced difference at finite isospin asymmetry ($I_a = 0.3$) in the magnitude of the δ field comparing to other fields. Unlike σ and ζ fields, the magnitude of δ field increases with baryon density, being largest at $\rho_B = \rho_0$, and it reflects the enhanced isospin splitting effects. The δ field is also moderately sensitive to strangeness fraction. At $\frac{\rho_0}{2}$ and $I_a = 0.3$, the δ field changes from -0.957 to -0.960 MeV as f_s is increased from 0.3 to 0.7. Thus, the magnetic response of the scalar fields are

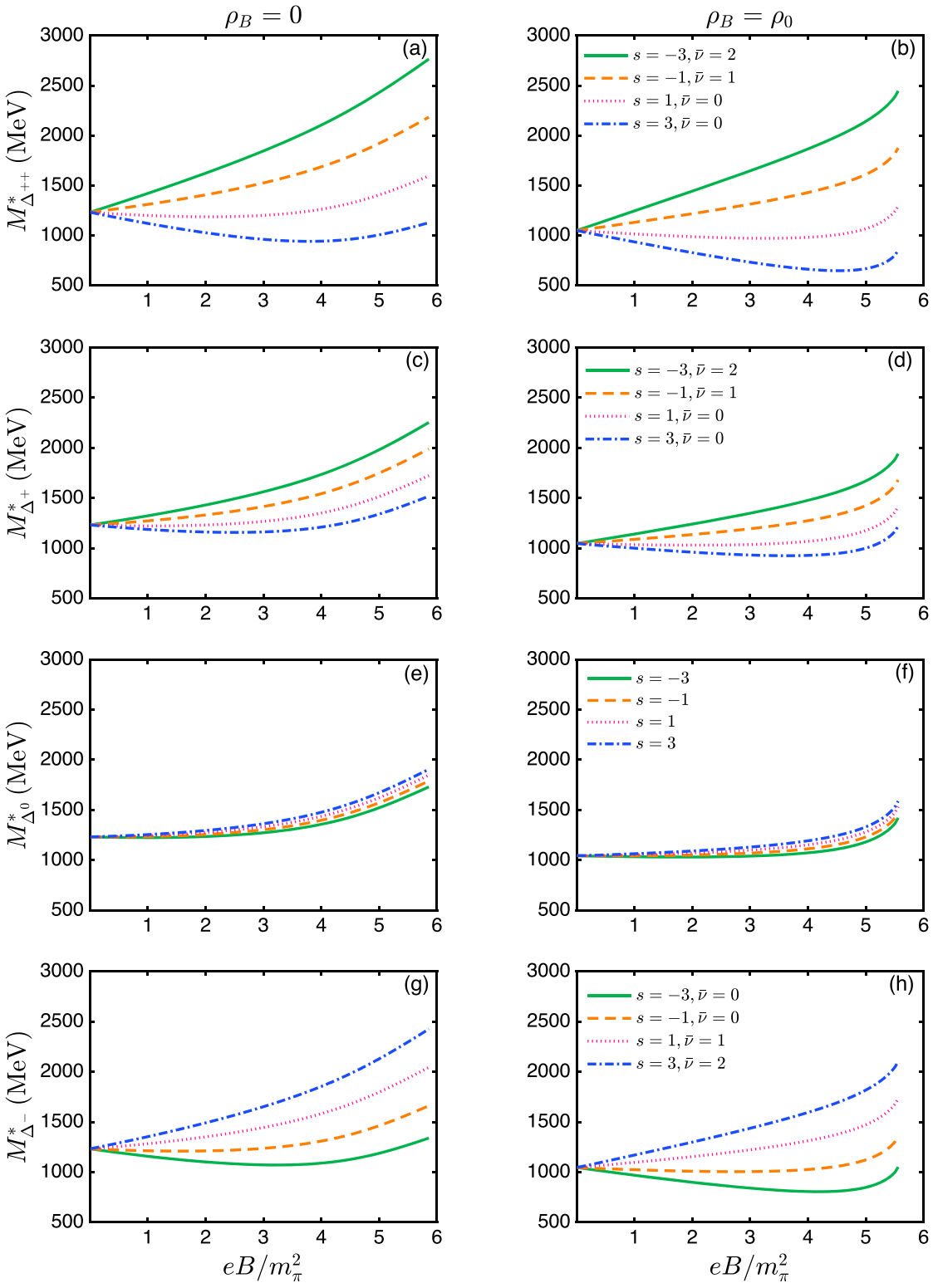


FIG. 2. Variation of effective masses of the Δ^{++}, Δ^{+}, Δ^{-}, and Δ^{0} baryons as a function of the magnetic field eB/m_π^2 for $f_s = 0.3$ and $I_a = 0.3$ at $\rho_B = 0$ [panels (a), (c), (e), and (g)] and $\rho_B = \rho_0$ [panels (b), (d), (f), and (h)] and T=100 MeV. The four curves in each panel correspond to the spin projections $s = -3, -1, 1$, and 3.

density dominated, with strangeness and isospin asymmetry acting as a secondary factor.

B. In-medium masses of decuplet baryons

In this section, we discuss the behavior of the effective masses of the decuplet baryons within the magnetized strange matter. Figures 2–4 show the in-medium masses of the decuplet baryons for different spin projections as a function of the magnetic field eB/m_π^2. The results of in-medium masses shown here are calculated using Eqs. (28) and (29). Figure 2 is for $\Delta^{++,+,0,-}$ and Fig. 3 for $\Sigma^{*+,0,-}$, whereas in Fig. 4 effective masses of $\Xi^{*0,-}$ and Ω^- baryons are shown. The results are presented for baryonic densities $\rho_B = 0$ (left panel) and $\rho_B = \rho_0$ (right panel), with isospin asymmetry $I_a = 0.3$, strangeness fraction $f_s = 0.3$, and temperature $T = 100$ MeV. In the case of positively charged baryons, for the spin projection $s = +3, +1$, and the lowest Landau level corresponds to the quantum number $\bar{\nu} = 0$, whereas for $s = -3$ and -1, $\bar{\nu}$ takes values 2 and 1, respectively [101]. For negatively charged baryons, for $s = -3, -1$, $\bar{\nu} = 0$ is the lowest, and for $s = +3$ and $+1$, $\bar{\nu}$ takes values 2 and 1, respectively.

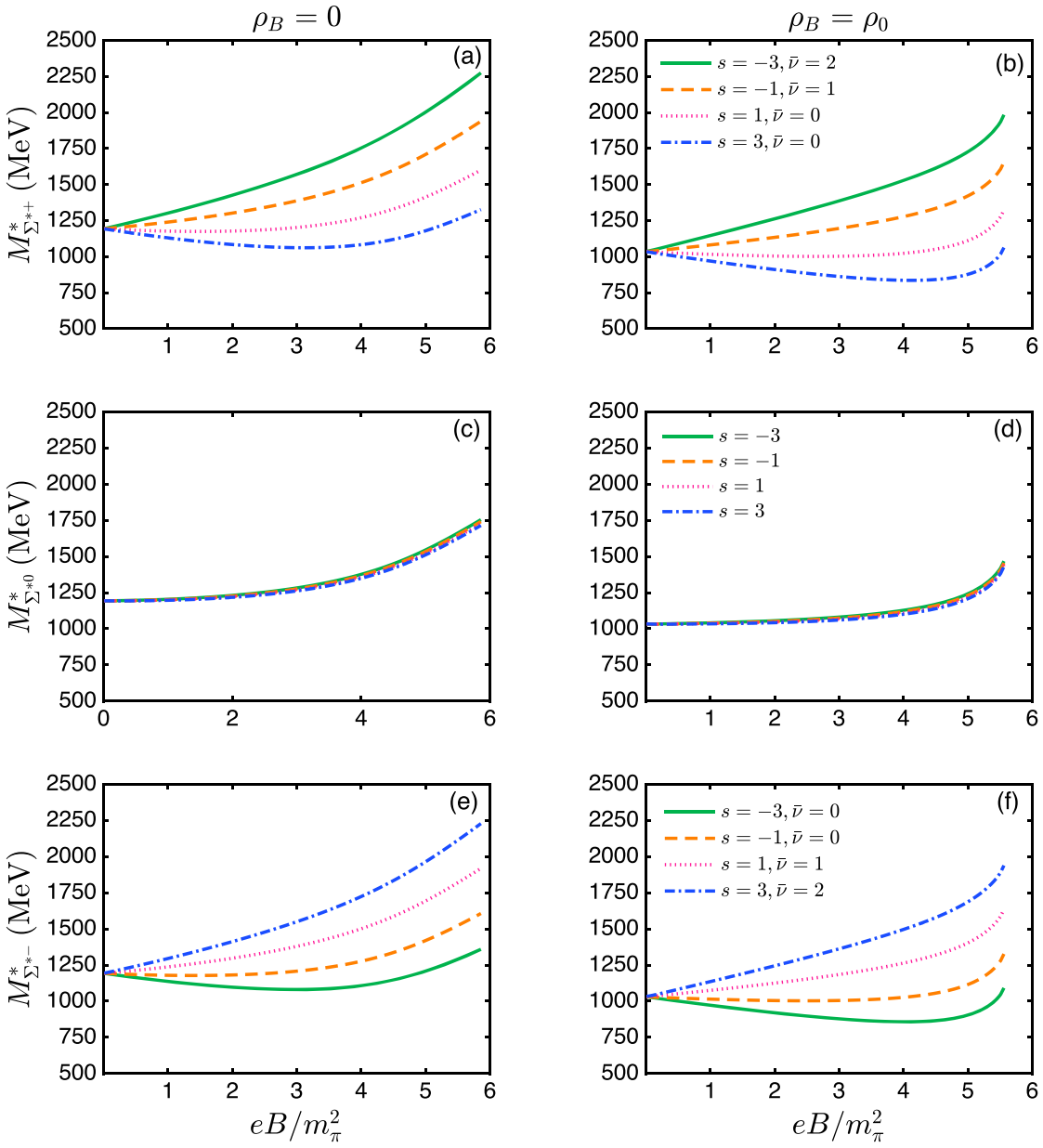


FIG. 3. Variation of effective masses of the Σ^{*+}, Σ^{*0}, and Σ^{*-} baryons as a function of the magnetic field eB/m_π^2 for $f_s = 0.3$ and $I_a = 0.3$ at $\rho_B = 0$ [panels (a), (c), and (e)] and $\rho_B = \rho_0$ [panels (b), (d), and (f)] and $T = 100$ MeV. The four curves in each panel correspond to the spin projections $s = -3, -1, 1$, and 3.

As observed from Fig. 2, the masses of Δ baryons corresponding to all spin projections originate near a common value in the absence of a magnetic field, while the splitting between the different spin states increases with increasing magnetic field depending on charge of the particle. In Fig. 2(a), the masses corresponding to the spin projections $s = -3$ and $s = -1$ of the Δ^{++} baryon increase monotonically with increasing magnetic field. Whereas the masses corresponding to $s = +3$ and $s = +1$, which occupy the lowest Landau level, initially decrease with increasing magnetic field and subsequently increase at higher magnetic fields. This arises due to the contributions of Landau level and AMM term given in Eq. (28). For the first Landau level $\bar{\nu} = 0$, the AMM contribution is the dominant magnetic field dependent term at low magnetic fields. Consequently, the AMM term causes the effective mass to decrease initially. However, at higher magnetic fields, the magnetic catalysis of the σ field becomes dominant, leading to an increase in the effective mass. Therefore, the lowest mass of Δ^{++} baryon is when spin $s = +3$ and highest for $s = -3$. As we increase the density from $\rho_B = 0$ to ρ_0, the mass of Δ^{++} baryon decreases by 14.64% for all spin projections at zero magnetic field as observed from Figs. 2(a) and 2(b). With a further increase in the magnetic field to $eB = 5.5m_\pi^2$, the mass decreases by 8.81%, 11.93%, 17.66%, and 24.91% for spin projections $s = -3$, -1, $+1$, and $+3$, respectively, relative to their corresponding values at $\rho_B = 0$, as shown in Fig. 2b). A similar trend can be seen from Figs. 2(c) and 2(d) for Δ^+ baryon. As discussed for Δ^{++} baryon, the masses of Δ^+ baryon for all four spin projections originate from a common point corresponding to the vacuum mass of Δ baryons. Whereas the masses of Δ^+ baryon corresponding to the spin projections occupying the lowest Landau level ($s = +1$ and $+3$), initially decrease by 0.77% and 5.99%, respectively, and subsequently increase, reaching overall increases of 32.6% and 17%, respectively, as the magnetic field reaches $eB = 5.5m_\pi^2$ from their value of mass at zero magnetic field as observed from Fig. 2(c). With the increase in density to ρ_0, as depicted in Fig. 2(d), the mass of Δ^+ baryon decreases by 14.8% at zero magnetic field, which is similar to Δ^{++} baryon. Panels (e) and (f) of Fig. 2 show the variation of the Δ^0 baryon mass with magnetic field for $\rho_B = 0$ and ρ_0, respectively. Since the Δ^0 baryon is neutral, it does not undergo Landau quantization. The four spin projections remain degenerate at zero magnetic field, while increasing magnetic field induces a relatively small mass splitting of 176 MeV, in contrast to the significantly larger spin-dependent mass variations of 1637.99 and 734.99 MeV for the Δ^{++} and Δ^+ baryons, respectively, between $s = -3$ and $s = +3$ at the same magnetic field and zero density. Unlike the positively charged Δ baryons, the Δ^0 baryon exhibits its lowest mass at $s = -3$, a behavior similar to that of the Δ^- baryon shown in Figs. 2(g) and 2(h). In Fig. 2(g), we observe that the spin projections $s = +1$ and $+3$ of Δ^- baryon occupy $\bar{\nu} = 1$ and 2, respectively, and the masses of Δ^- baryon increase monotonically with magnetic field by 57.3% and 86.5% at $eB = 5.6m_\pi^2$ from the value at zero magnetic field. Whereas the masses of Δ^- baryon for which lower Landau level $\bar{\nu} = 0$ is occupied by $s = -1$ and -3 initially decreases reaching a minimum value at $eB = 3.2m_\pi^2$ and then increases rapidly by 3.3% from the value at zero magnetic field. As moving to higher density, the mass of Δ^- baryon decreases for all spin projections as discussed for other Δ baryons.

In Fig. 3, we discuss the in-medium masses for $\Sigma^{*+,0,-}$ baryons for all four spin projections. From Fig. 3(a), we observe that the mass of Σ^{*+} baryon for all spin originate near 1193 MeV at zero magnetic field with $s = -3$ and -1 ($\bar{\nu} \geq 1$) increasing monotonically by 89.2% and 61.2%, respectively, as magnetic field reaches $eB = 5.5m_\pi^2$. While $s = +1$ and $+3$ ($\bar{\nu} = 0$), the mass of Σ^{*+} baryon decreases first and later increases by 27.4% and 5.8%, respectively, at $eB = 5.5m_\pi^2$. The density dependence of the Σ^{*+} baryon mass exhibits a behavior similar to that observed for the Δ baryons. As the baryon density increases from $\rho_B = 0$ to ρ_0, the mass of the Σ^{*+} baryon decreases by 158.73 MeV, as shown in Fig. 3(b). Whereas the neutral Σ^{*0} baryon does not undergo Landau quantization, and its four spin states remain nearly degenerate throughout the variation of the magnetic field, with a maximum splitting of 39.45 MeV between the $s = -3$ and $s = +3$ states as depicted in Fig. 3(c). Unlike the Δ^0 baryon, the $s = -3$ state exhibits the highest mass, while the $s = +3$ state has the lowest mass, indicating an opposite sign of the effective AMM coupling. Moreover, the mass of the Σ^{*0} baryon increases monotonically with the magnetic field for all spin projections. With increasing baryon density, the mass of the Σ^{*0} baryon decreases, while its variation with the magnetic field becomes progressively weaker at higher densities as observed from Fig. 3(d). In Figs. 3(e) and 3(f), we observe the splitting of the Σ^{*-} baryon masses for different s, following a trend similar to that observed for the Σ^{*+} baryon but with an opposite dependence on s. At $\rho_B = 0(\rho_0)$, the masses of Σ^{*-} baryon corresponding to $s = +1$ and $+3$ increase with the magnetic field, reaching increases of 52.6% and 77.2% (53.8% and 83.1%), respectively, relative to their values at zero magnetic field, at $eB = 5.5m_\pi^2$. Whereas the masses for $s = -3$ and -1 initially decrease by 1.27% and 9.35% (2.78% and 16.82%), respectively, before increasing with the magnetic field.

In Fig. 4, we plot the in-medium masses of the Ξ^{*0}, Ξ^{*-}, and Ω^- baryons for all spin projections with magnetic field. From Fig. 4(a), the masses of the Ξ^{*0} baryon for all spin projections originate near 1317.6 MeV at zero magnetic field. With an increase in magnetic field, the mass of Ξ^{*0} baryon is observed to increase for all s. Since the Ξ^{*0} baryon carries no electric charge, it does not undergo Landau quantization, and its four spin states remain nearly

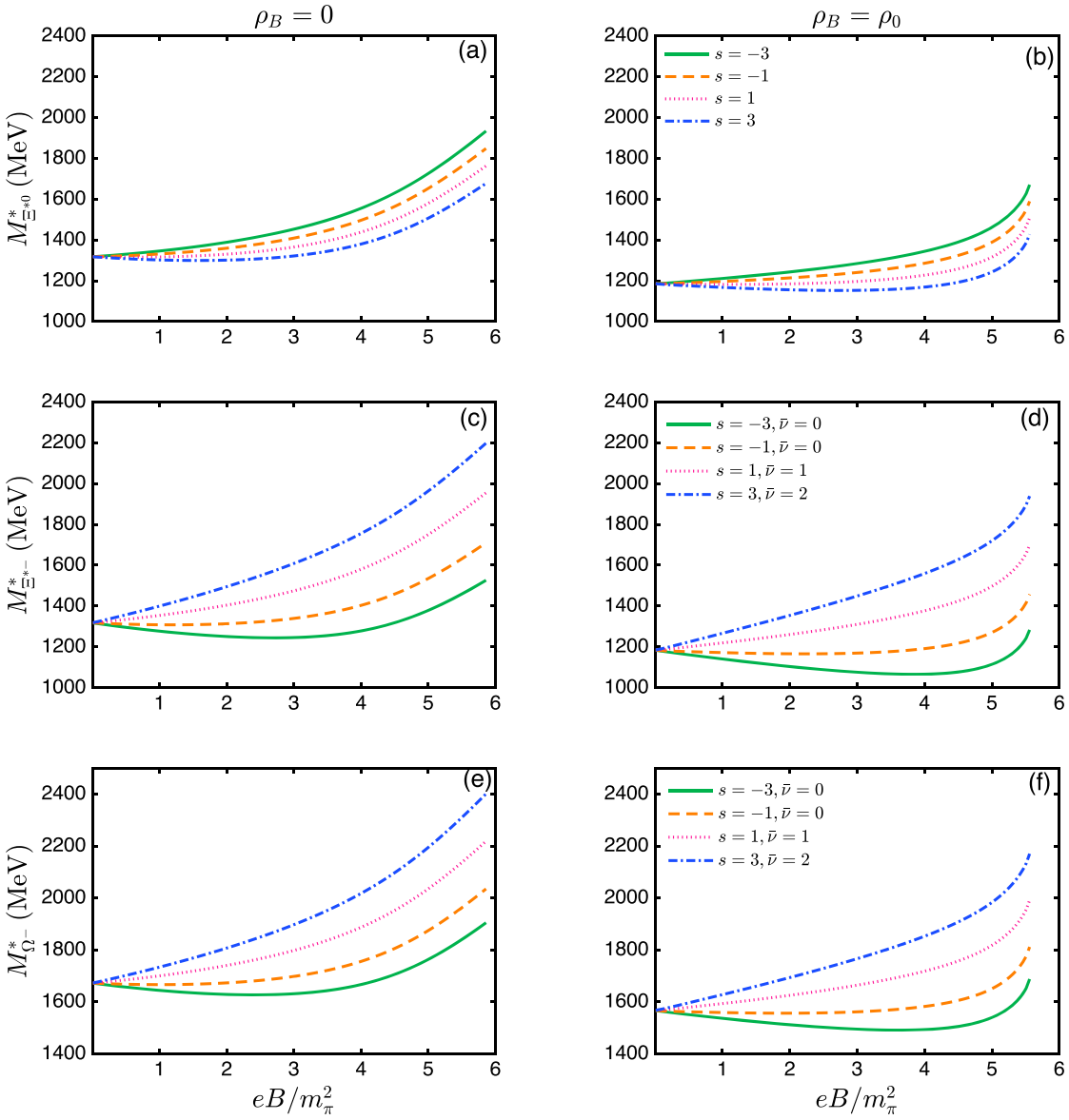


FIG. 4. Variation of effective masses of the Ξ^{*0}, Ξ^{*-}, and Ω^- baryons as a function of the magnetic field eB/m_π^2 for $f_s = 0.3$ and $I_a = 0.3$ at $\rho_B = 0$ [panels (a), (c), and (e)] and $\rho_B = \rho_0$ [panels (b), (d), and (f)] at $T = 100$ MeV. The four curves in each panel correspond to the spin projections $s = -3, -1, 1$, and 3.

degenerate up to $eB \approx 1m_\pi^2$, reaching a maximum splitting of 241.15 MeV between the $s = -3$ and $s = +3$ states at $eB = 5.5m_\pi^2$. Similar to Σ^{*0}, the $s = -3$ state has the largest mass, while the $s = +3$ state has the smallest mass. As the density increases from $\rho_B = 0$ to ρ_0, the mass decreases by 131.67 MeV at zero magnetic field, as shown in Fig. 4(b). From Figs. 4(c) and 4(d), we can see that the Ξ^{*-} baryon follows the same trend as observed for the negatively charged Δ^- and Σ^{*-} baryons. The masses of the Ξ^{*-} baryon corresponding to the spin projections $s = +1$ and $+3$ ($\bar{\nu} \geq 1$) increase monotonically with the magnetic field, reaching 41.6% and 59.1%, respectively, at $eB = 5.5m_\pi^2$ for $\rho_B = 0$. But, the masses for $s = -3$ and -1 states ($\bar{\nu} = 0$) initially decrease by 5.54% ($eB = 2.7m_\pi^2$) and 0.73% ($eB = 1.2m_\pi^2$), respectively, before increasing again as discussed for other negatively charged baryons. As the density increases from $\rho_B = 0$ to ρ_0, the mass decreases in between 133.46–133.49 MeV for all spin projections at zero magnetic field.

From Figs. 4(e) and 4(f), the Ω^- baryon, which consists entirely of strange quarks, exhibits the weakest magnetic field response in the entire decuplet. The masses of Ω^- baryon corresponding to spin projections $s = +1$ and $+3$ increase with increase in magnetic field. Whereas the masses of Ω^- baryon for $s = -3$ and -1 states initially decreases to 1626.78 and 1666.24 MeV at $eB = 2.4m_\pi^2$ and $eB = 1.1m_\pi^2$, respectively, from its mass value 1672.59 MeV at zero magnetic field as depicted in

Fig. 4(e). From Fig. 4(f), as the density increases from $\rho_B = 0$ to ρ_0, the mass decreases by 105.07 MeV at zero magnetic field, which is the smallest density induced shift among all the baryons in the decuplet.

To further understand the impact of baryon density, strangeness fraction, and isospin asymmetry of the medium, in Figs. 5–7 we illustrate the dependence of the effective masses of the decuplet baryons on the magnetic

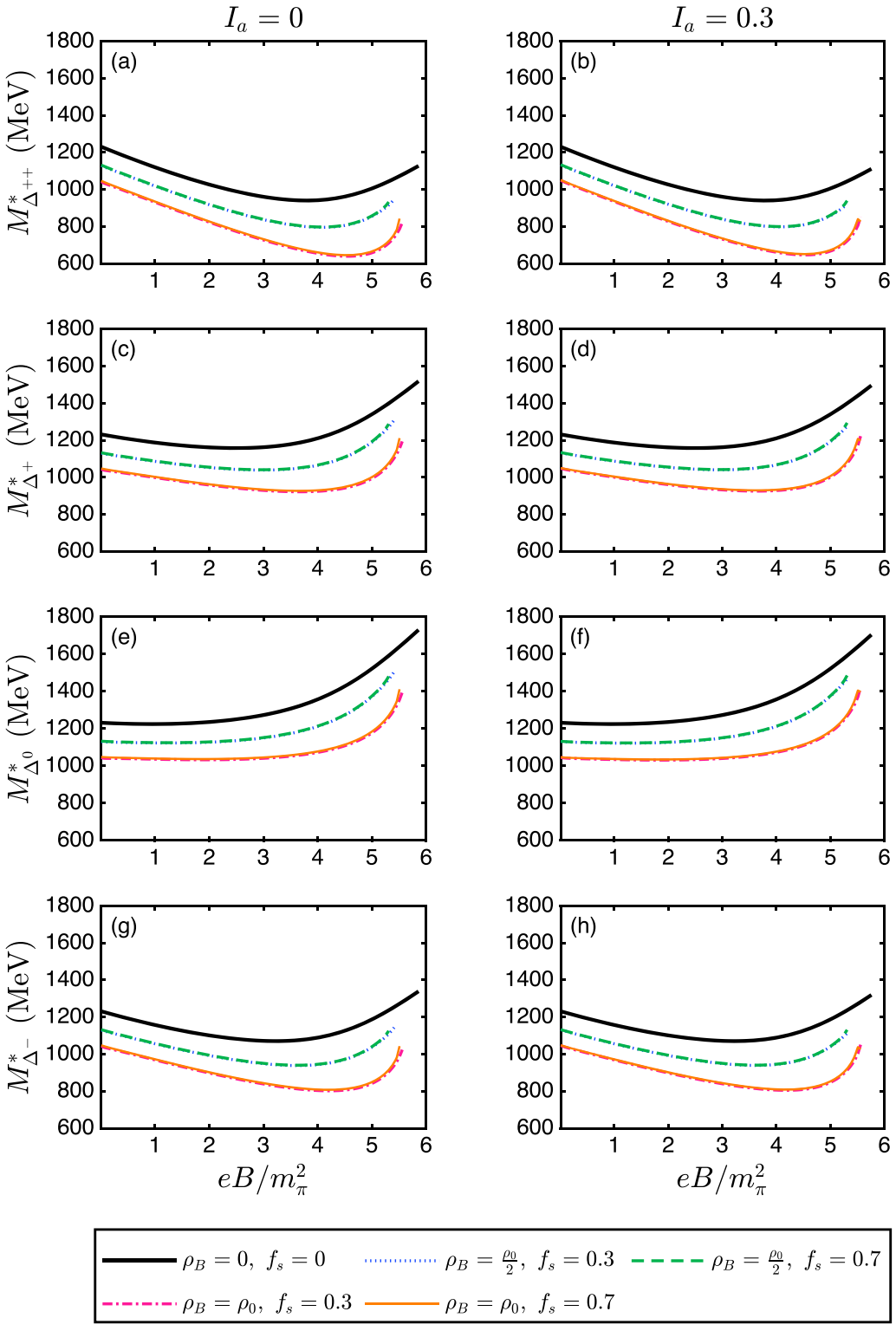


FIG. 5. Variation of masses of Δ baryons with magnetic field eB/m_π^2 for isospin symmetric $I_a = 0$ [panels (a), (c), (e), and (g)] and isospin asymmetric $I_a = 0.3$ [panels (b), (d), (f), and (h)] at $T = 100$ MeV. Each panel shows the result corresponding to different baryonic density ρ_B and strangeness fraction f_s.

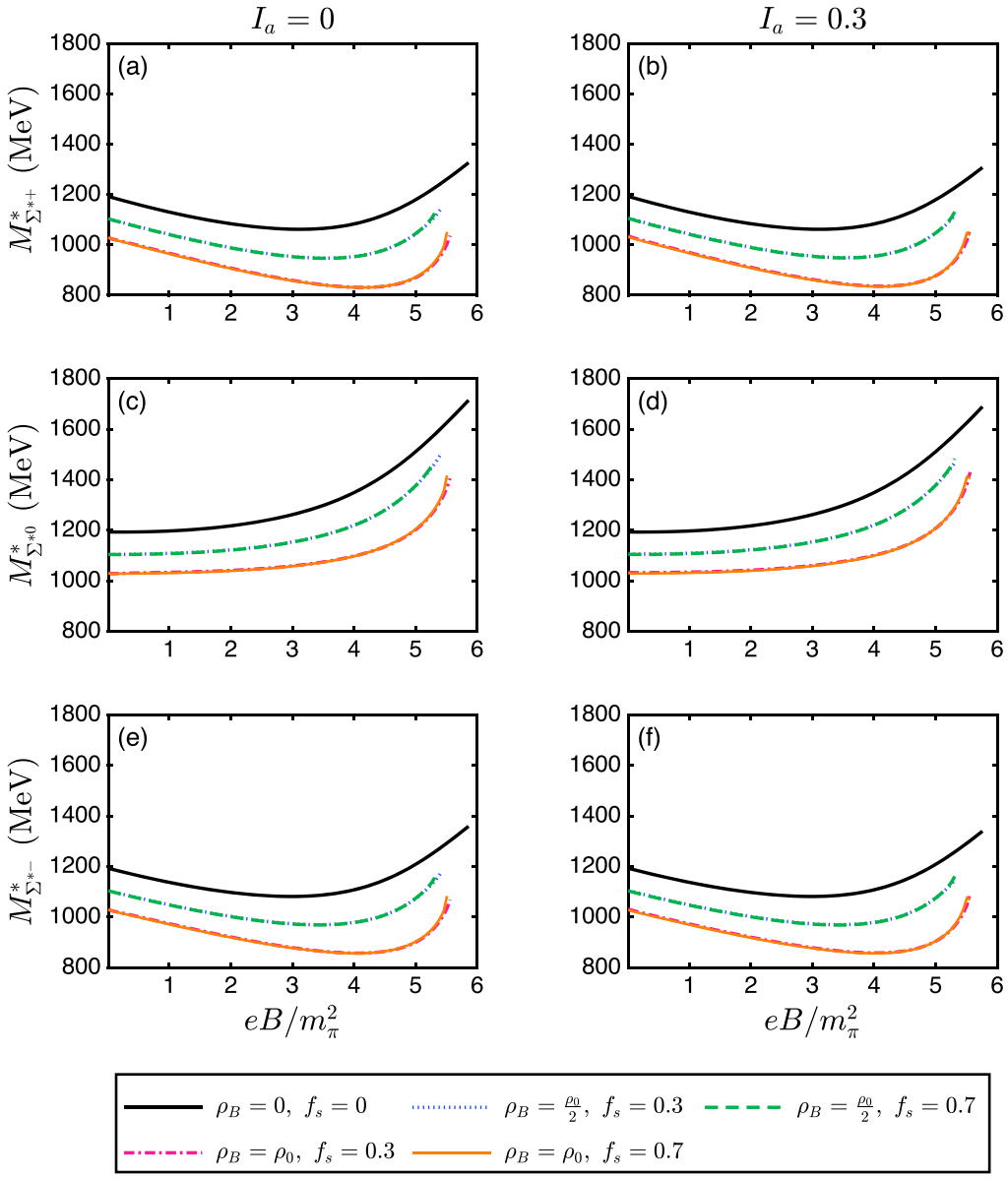


FIG. 6. Variation of masses of Σ^* baryons with magnetic field eB/m_π^2 for isospin symmetric $I_a = 0$ [panels (a), (c) and (e)] and isospin asymmetric $I_a = 0.3$ [panels (b), (d), and (f)] at $T = 100$ MeV. Each panels shows the result corresponding to different baryonic density ρ_B, strangeness fraction f_s.

field eB/m_π^2 for different baryonic densities ($\rho_B = 0, \frac{\rho_0}{2}, \rho_0$) and strangeness fractions ($f_s = 0, 0.3, 0.7$), at isospin asymmetries $I_a = 0$ (left panel) and $I_a = 0.3$ (right panel), for temperature $T = 100$ MeV. For each baryon, the results are shown for the spin projection s and Landau level $\bar{\nu}$ corresponding to the lowest effective mass. For a quantitative comparison, the in-medium masses of the decuplet baryons at different values of magnetic fields eB/m_π^2, baryonic densities ρ_B, with $f_s = 0.3$ and $T = 100$ MeV are tabulated in Tables III (for $I_a = 0$) and IV (for $I_a = 0.3$).

In Fig. 5, we have shown the variation of effective masses of Δ baryons in magnetized strange matter as a function of eB/m_π^2 for different baryonic densities ρ_B and strangeness fraction f_s. For symmetric matter ($I_a = 0$), shown in Figs. 5(a), 5(c), 5(e), and 5(g), the effective mass of the Δ baryon initially decreases with increasing magnetic field and subsequently increases at all baryonic densities and strangeness fraction. However, the rate of decrease in the mass of the Δ^0 baryon is much smaller, since it does not undergo Landau quantization, and it starts to increase as the magnetic field reaches $1.5 - 2m_\pi^2$. The initial decrease in the effective mass is due to the effects of AMM and Landau quantization as discussed earlier. As the magnetic field increases further, magnetic catalysis enhances the σ field, leading to an increase in the effective mass. As we increase the density from $\rho_B = 0$ to $\frac{\rho_0}{2}$ and ρ_0, the mass decreases for all Δ baryons. The influence of f_s is weaker for the Δ baryons, since they do not contain strange

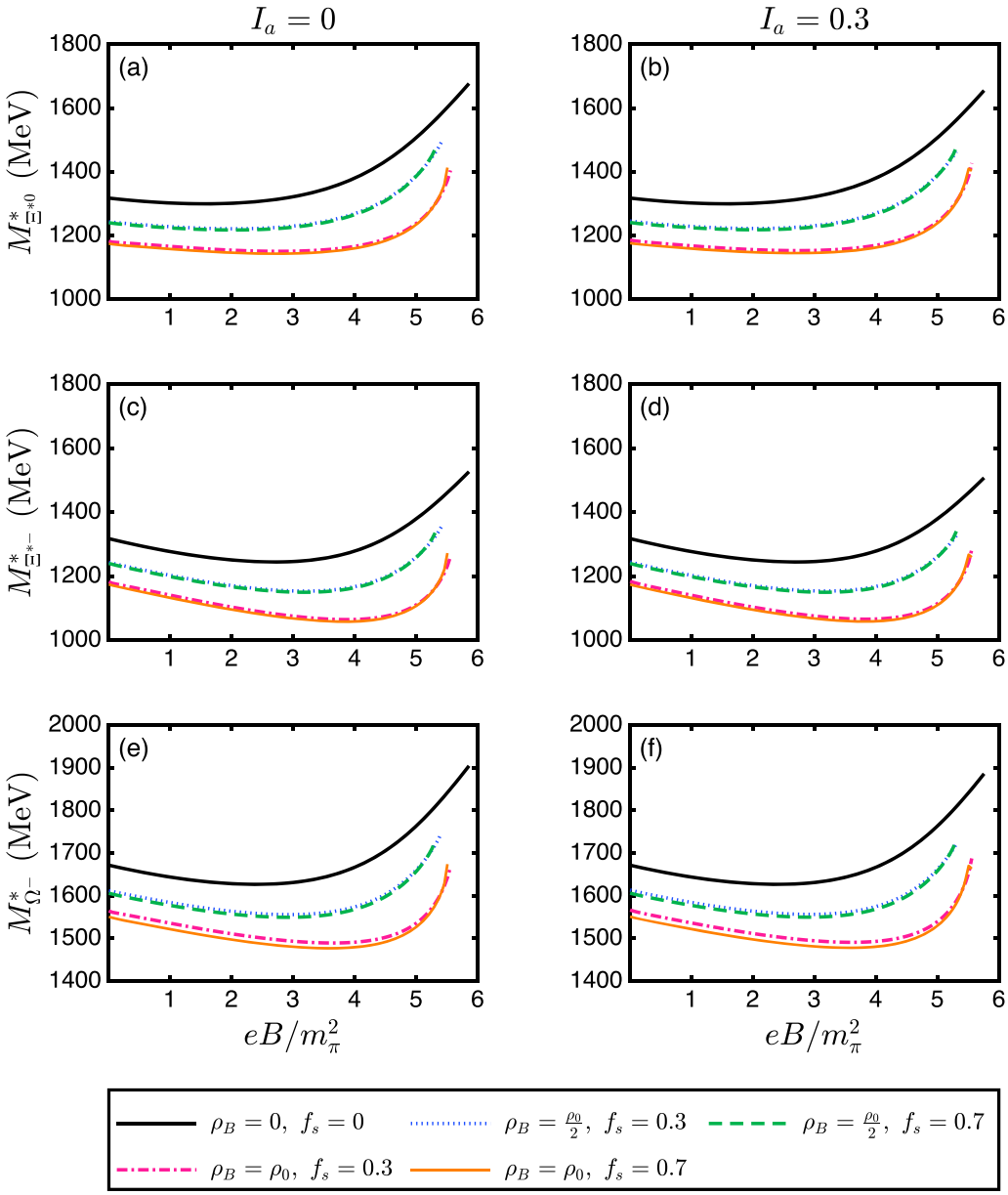


FIG. 7. Same as Fig. 5, for Ξ^* baryons [panels (a), (b), (c), and (d)] and Ω^- baryons [panels (e) and (f)].

quarks. For isospin asymmetric matter ($I_a = 0.3$), a similar trend is observed as in the isospin symmetric medium, as shown in Figs. 5(b), 5(d), 5(f), and 5(h). However, the effective mass of the Δ baryons exhibits an isospin-dependent splitting. At zero magnetic field, the mass of the Δ^{++} baryon increases by about 4.79 MeV for $\rho_B = \rho_0$ and $f_s = 0.7$ when the isospin asymmetry is increased from $I_a = 0$ to $I_a = 0.3$. This enhancement gradually decreases as one moves from Δ^{++} to Δ^-. Consequently, the Δ^- baryon shows the opposite behavior, with its effective mass becoming slightly lower for $I_a = 0.3$ than for $I_a = 0$.

In Figs. 6(a) and 6(e), for isospin symmetric matter ($I_a = 0$), the effective masses of the charged Σ^{*+} and Σ^{*-} baryons initially decrease with increasing magnetic field and later they increase with further increase in magnetic field. This behavior is similar to that observed for the charged Δ baryons. Furthermore, with increasing baryon density from $\rho_B = 0$ to ρ_0, the overall magnitude of the effective masses decreases owing to the enhanced scalar fields in the medium. In contrast, the Σ^{*0} baryon carries no electric charge; it does not experience Landau quantization resulting in a gradual increase in the effective mass with increasing magnetic field as illustrated in Figs. 6(c) and 6(d). As discussed for Δ baryons isospin dependence is observed for Σ^* baryons as I_a increases from 0 to 0.3, with the masses of Σ^{*+}, Σ^{*0}, and Σ^{*-} baryons increasing by 4.67, 2.71, and 0.74 MeV, respectively, at $\rho_B = \rho_0$, $f_s = 0.3$, and $eB = 0$. The dependence on f_s is stronger than that of the Δ baryons but remains relatively weak due to the presence of only one strange quark.

TABLE III. Effective masses of decuplet baryons (in MeV) at different magnetic fields eB/m_π^2, baryon densities ρ_B, strangeness fraction $f_s = 0.3$, isospin asymmetry $I_a = 0$, and temperature $T = 100$ MeV.

	$\rho_B = \frac{\rho_0}{2}$			$\rho_B = \rho_0$		
Baryon	$eB = 0\ m_\pi^2$	$eB = 3\ m_\pi^2$	$eB = 5\ m_\pi^2$	$eB = 0\ m_\pi^2$	$eB = 3\ m_\pi^2$	$eB = 5\ m_\pi^2$
Δ^{++}	1128.83	836.68	856.56	1043.32	726.59	659.38
Δ^{+}	1129.57	1039.07	1191.94	1044.12	929.21	995.33
Δ^{-}	1129.33	948.18	1039.15	1043.95	838.54	843.12
Δ^{0}	1130.07	1150.57	1374.53	1044.75	1041.16	1179.07
Σ^{*+}	1103.80	953.48	1045.46	1030.24	858.29	870.96
Σ^{*-}	1104.00	972.90	1074.79	1030.57	878.17	901.44
Σ^{*0}	1104.53	1154.00	1377.73	1031.04	1059.05	1203.81
Ξ^{*-}	1242.88	1153.70	1260.81	1182.39	1074.89	1111.17
Ξ^{*0}	1243.07	1229.74	1388.87	1182.51	1150.69	1238.65
Ω^{-}	1612.06	1555.98	1661.52	1564.78	1493.45	1536.35

TABLE IV. Effective masses of decuplet baryons (in MeV) at different magnetic fields eB/m_π^2, baryon densities ρ_B, strangeness fraction $f_s = 0.3$, isospin asymmetry $I_a = 0.3$, and temperature $T = 100$ MeV.

	$\rho_B = \frac{\rho_0}{2}$			$\rho_B = \rho_0$		
Baryon	$eB = 0\ m_\pi^2$	$eB = 3\ m_\pi^2$	$eB = 5\ m_\pi^2$	$eB = 0\ m_\pi^2$	$eB = 3\ m_\pi^2$	$eB = 5\ m_\pi^2$
Δ^{++}	1133.08	838.90	860.33	1049.34	731.34	668.46
Δ^{+}	1132.84	1040.38	1194.98	1048.19	932.06	1002.68
Δ^{-}	1131.63	948.58	1041.46	1046.07	839.50	848.72
Δ^{0}	1131.40	1150.06	1376.11	1044.93	1040.22	1182.94
Σ^{*+}	1107.19	955.14	1048.59	1034.91	861.87	878.42
Σ^{*-}	1105.43	972.74	1076.46	1031.31	877.93	905.40
Σ^{*0}	1106.95	1154.76	1380.13	1033.75	1060.72	1209.52
Ξ^{*-}	1244.40	1153.90	1262.55	1183.70	1075.36	1115.18
Ξ^{*0}	1245.56	1230.84	1391.34	1185.77	1153.06	1244.40
Ω^{-}	1613.66	1556.52	1663.32	1566.62	1494.60	1540.38

In panels (a), (b), (c), and (d) of Fig. 7, we discuss the masses of Ξ^* baryons. For isospin symmetric matter ($I_a = 0$), the neutral Ξ^{*0} baryon exhibits a behavior similar to that of the neutral Δ^0 baryon, as illustrated in Fig. 7(a). Since the Ξ^{*0} carries no electric charge, the effective mass decreases negligibly with increasing magnetic field up to $eB = 1.5$–$2m_\pi^2$ after which it increases rapidly. Whereas with the charged Ξ^{*-} baryon the effective mass decreases significantly at low magnetic fields and subsequently increases, as shown in Fig. 7(c). The influence of isospin asymmetry on the Ξ^* baryons is weak because of the presence of only one light quark. Increasing I_a from 0 to 0.3 increases the mass of Ξ^{*0} by 0.88 MeV, while that of Ξ^{*-} decreases by 0.13 MeV, as evident from Figs. 7(a)–7(d) and Tables III and IV. This weak dependence arises because only the light quark couples to the isovector δ field, while the two strange quarks remain unaffected. The dependence on f_s is slightly stronger due to the presence of two strange quarks. For example, increasing f_s from 0.3 to 0.7 decreases the Ξ^{*-} mass by 7.81 MeV at $\rho_B = \frac{\rho_0}{2}$ and $eB = 3m_\pi^2$.

Panels (e) and (f) in Fig. 7 show the magnetic field dependence of mass of Ω^- baryon. As shown in Figs. 7(e) and 7(f), the mass of Ω^- baryon initially decreases and subsequently increases rapidly, similar to the other charged decuplet baryons. Furthermore, increasing the baryon density from $\rho_B = 0$ to $\frac{\rho_0}{2}$ and ρ_0 leads to a reduction in the overall magnitude of the effective mass. The isospin dependence is very weak since the Ω^- baryon contains only strange quarks, whereas its f_s dependence is stronger because all three quarks couple to the strange scalar field ζ. For example, increasing f_s from 0.3 to 0.7 decreases its mass by 7.52 MeV for $\rho_B = \frac{\rho_0}{2}$ at $eB = 0$ and $I_a = 0$, as given in Fig. 7(e).

Previous studies of spin-$\frac{3}{2}$ Δ baryons have shown that Landau quantization leads to spin-dependent distribution among allowed Landau levels, while the inclusion of AMMs further enhances the different spin projections in strong magnetic fields [101]. The existing studies on decuplet baryon masses are found to decrease monotonically with increasing baryonic density consistent with previous CQMF

studies in symmetric nuclear and hyperonic matter [56–58]. The role of isospin asymmetry in the medium has been studied using the CQMF model in Refs. [55,81], where the scalar-isovector field δ is found to induce charge state splitting among the multiplet members, with the splitting being most pronounced for baryons composed entirely of light quarks. The inclusion of Dirac sea contributions are essential for magnetic catalysis of scalar condensates in magnetized matter [42,44–46], and at the quark level, the enhancement of the scalar condensate σ with increasing magnetic field is due to the phenomenon of magnetic catalysis of chiral symmetry breaking established in Refs. [16,17], where a constant magnetic field acts as a catalyst of dynamical chiral symmetry breaking. The present findings are consistent with the existing results mentioned above.

C. In-medium magnetic moments of decuplet baryons

In this section, we present the results of magnetic moments of decuplet baryons and their behavior in magnetized strange matter. The total effective magnetic moment is calculated as the sum of the valence, sea, and orbital contributions of the quarks, as given in Eq. (32), with the individual contributions evaluated using Eq. (33). The effective magnetic moment of baryons depend upon the effective magnetic moments of constituent quarks calculated using Eqs. (34) and (35) as well as in-medium mass of baryon obtained from Eqs. (28) and (29). As discussed in the previous section, in the presence of finite magnetic field, the in-medium mass of decuplet baryon splits due to finite anomalous magnetic moment term as the spin projection s takes the values ± 3 and ± 1. For the calculations of magnetic moment of baryons, we consider the baryon mass corresponding to the value of s which gives lowest mass as a function of magnetic field. Figures 8–10 show the variation of total effective magnetic moment and the individual contributions of valence, sea, and orbital angular momentum of sea quarks of decuplet baryons with magnetic field for different baryonic densities $\rho_B = \frac{\rho_0}{2}$ (left panel) and $\rho_B = \rho_0$ (right panel) at strangeness fraction $f_s = 0.7$ and isospin asymmetry $I_a = 0.3$, including the total magnetic moment at $\rho_B = 0$, $f_s = 0$, and $I_a = 0$ for comparison. Tables V, VI, and VII show the values of magnetic moments of all decuplet baryons at different baryonic densities, strangeness fraction, and isospin asymmetry for different values of magnetic field.

Figure 8 shows the variations of magnetic moment of Δ baryons with magnetic field. From Fig. 8(a), we observe that at $\rho_B = \frac{\rho_0}{2}$ the valence contribution to the magnetic moment of Δ^{++} baryon is dominant and positive ($9.468\mu_N$), primarily driving the total baryon magnetic moment, while the sea contribution is negative ($-1.969\mu_N$), and the orbital contribution is positive but comparatively small ($0.511\mu_N$) at zero magnetic field. Due to the effect of these three contributions, the net magnetic moment at zero magnetic field turns out to be $8.011\mu_N$ at $\rho_B = \frac{\rho_0}{2}$, whereas the value of total magnetic moment is $6.464\mu_N$ at vacuum, i.e., $\rho_B = 0, f_s = 0$ and $I_a = 0$. With an increase in magnetic field, the total magnetic moment of Δ^{++} increases until $eB = 2.96m_\pi^2$ ($9.570\mu_N$) and later decreases with further increase in magnetic field as depicted in Fig. 8(a). As shown in Fig. 8(b), when the baryon density is increased from $\rho_B = \frac{\rho_0}{2}$ to ρ_0, the overall trend remains similar to that observed for $\rho_B = \frac{\rho_0}{2}$. However, the total magnetic moment of the Δ^{++} baryon increases by $2.105\mu_N$ at zero magnetic field. This enhancement is due to the decrease in the effective baryon mass with increasing density, which consequently leads to an increase in the magnetic moment. Figures 8(c) and 8(d) show the variation of magnetic moment of Δ^+ baryon with magnetic field. As discussed for Δ^{++} baryon, the Δ^+ baryon also follows the same trend with magnetic field and has a positive total magnetic moment. With increase in density from $\rho_B = 0$ to $\frac{\rho_0}{2}$ and ρ_0, the total magnetic moment shifts from $2.801\mu_N$ to $3.591\mu_N$ and $4.756\mu_N$, respectively, at $eB = 3m_\pi^2$. The magnetic moment variation with density of D^+ baryon is also qualitatively similar to Δ^{++} baryon. As shown in Figs. 8(e) and 8(f), all three contributions to the magnetic moment of the Δ^0 baryon remain negative. Consequently, the total magnetic moment is also negative and is primarily governed by the sea quark contribution. Unlike Δ^{++} and Δ^+ baryons, the total magnetic moment at $\rho_B = 0$, $\rho_B = \frac{\rho_0}{2}$, and ρ_0 exhibits an opposite trend with increasing magnetic field. The magnitude of total magnetic moment of Δ^0 baryon at $\rho_B = 0$, $f_s = 0$, and $I_a = 0$ increases with magnetic field, whereas the magnitude total magnetic moment at finite densities decreases with magnetic field as depicted in Figs. 8(e) and 8(f). With an increase in the baryon density from $\rho_B = \frac{\rho_0}{2}$ to $\rho_B = \rho_0$, the magnitude of the total magnetic moment of the Δ^0 baryon increases by $0.146\mu_N$. The Δ^- baryon consists of three d quarks, resulting in a negative valence contribution leading to an overall negative total magnetic moment as shown in Figs. 8(g) and 8(h). With an increasing magnetic field, the magnitude of the total magnetic moment initially shows a small increase up to $eB = 2.85m_\pi^2$, beyond which it decreases. Following the trend observed for the other Δ baryons, the magnitude of magnetic moment of Δ^- baryon increases with increasing baryonic density as shown in Fig. 8(h).

Variation of magnetic moment of Σ^* baryons with magnetic field is depicted in Fig. 9. For Σ^{*+} baryons, as shown in Figs. 9(a) and 9(b), the two u quarks dominate, and therefore, valence contribution is large and positive compared to other contribution to the total magnetic moment. Therefore, the resulting total magnetic moment of the Σ^{*+} baryon remains positive and increases gradually up to $eB = 1.85m_\pi^2$, beyond which it starts to decrease with further increase in the magnetic field. As the density is increased to ρ_0, the magnitude of total magnetic

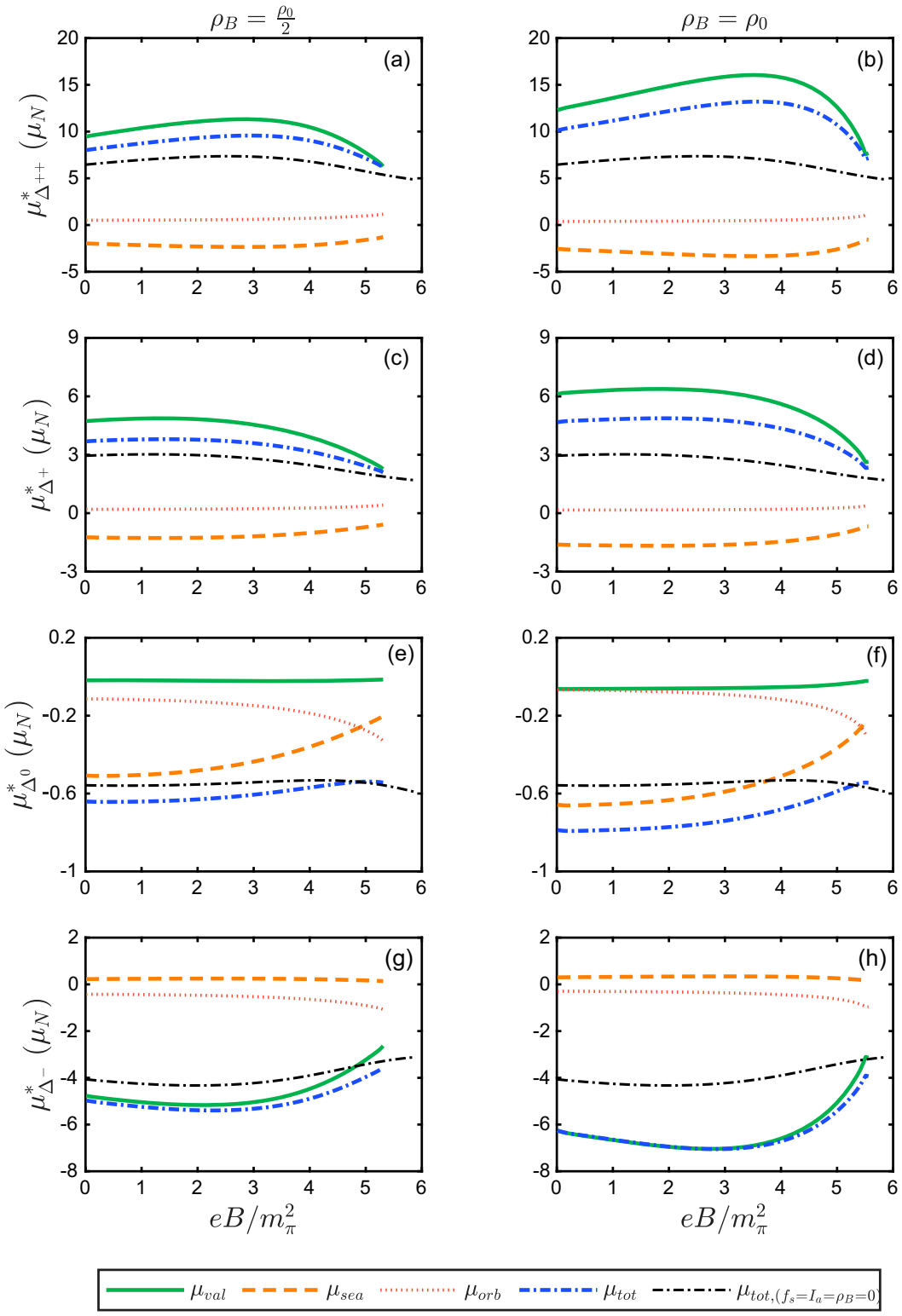


FIG. 8. In-medium magnetic moment variation of Δ baryons as a function of magnetic field eB/m_π^2 for density $\rho_B = \frac{\rho_0}{2}$ [panels (a), (c), (e), and (g)] and $\rho_B = \rho_0$ [panels (b), (d), (f), and (h)] at $f_s = 0.7$, $I_a = 0.3$, and T = 100 MeV. The black dash-dotted curve corresponds to the total magnetic moment calculated for $\rho_B = 0$, $f_s = 0$ and $I_a = 0$. Each panel shows the result corresponding to different contributions to magnetic moments.

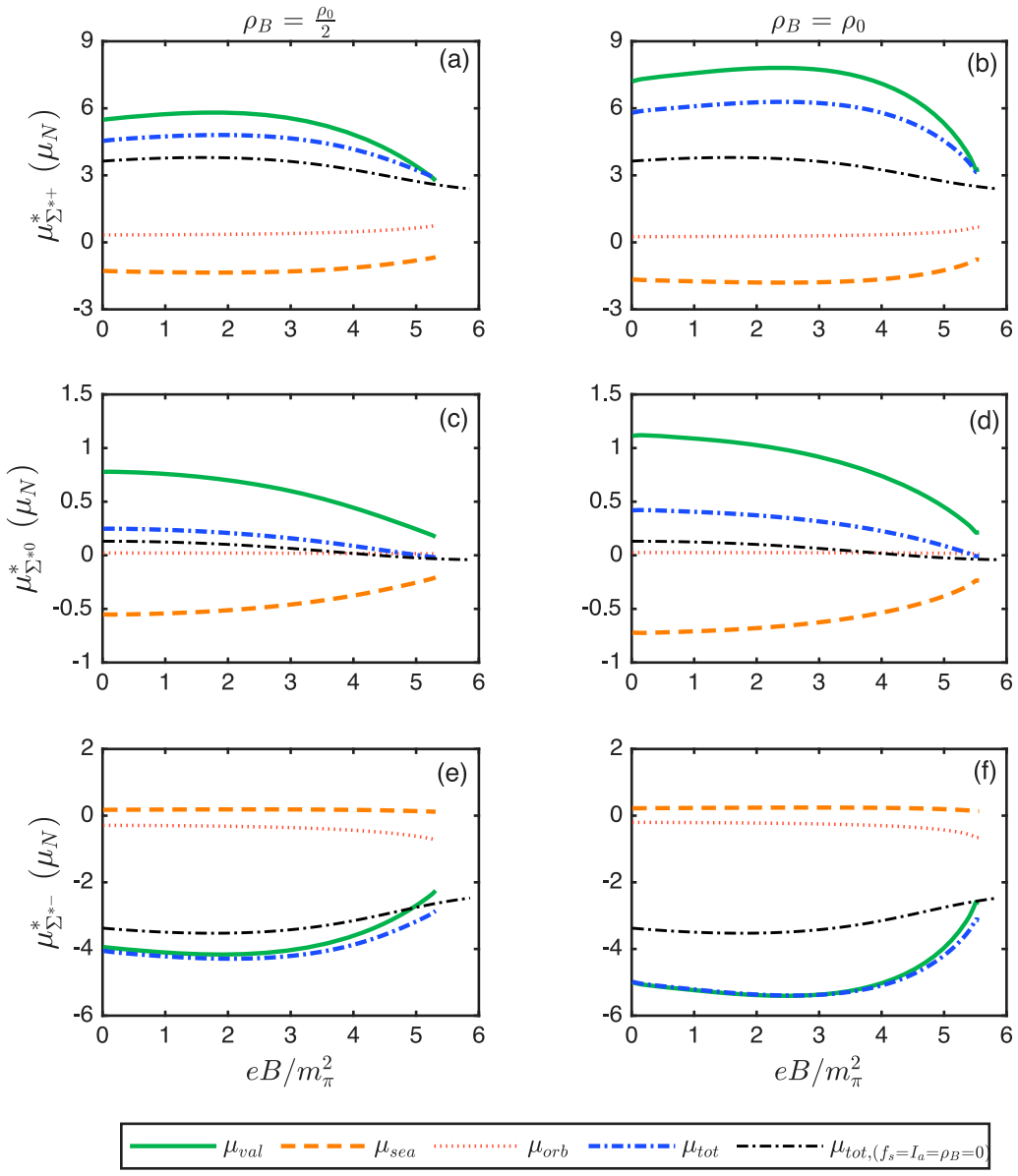


FIG. 9. In-medium magnetic moment variation of Σ^* baryons as a function of magnetic field eB/m_π^2 for density $\rho_B = \frac{\rho_0}{2}$ [panels (a), (c), and (e)] and $\rho_B = \rho_0$ [panels (b), (d), and (f)] at $f_s = 0.7$, $I_a = 0.3$ and $T = 100$ MeV. The black dash-dotted curve corresponds to the total magnetic moment calculated for $\rho_B = 0$, $f_s = 0$, and $I_a = 0$. Each panels shows the result corresponding to different contributions to magnetic moments.

moment of the Σ^{*+} baryon increases by a value $1.290\mu_N$ as shown in Figs. 9(a) and 9(b) at $eB = 5m_\pi^2$. For Σ^{*0} baryon in Figs. 9(c) and 9(d), the total magnetic moment decreases with increase in magnetic field reaching a negative value at higher magnetic field and as we increase the density from $\rho_B = 0$ to $\frac{\rho_0}{2}(\rho_0)$ the value of the total magnetic moment increases by $0.116(0.287)\mu_N$ which follows the same trend as Σ^{*+} baryon. Unlike the Σ^{*+} and Σ^{*0} baryons, the sea contribution to the magnetic moment of the Σ^{*-} baryon (dds) is small but positive, as shown in Figs. 9(e) and 9(f). However, the valence contributions from the two d quarks and the s quark are all negative, resulting in an overall negative total magnetic moment. The magnitude of the total magnetic moment increases gradually up to $eB = 2.05m_\pi^2$, beyond which it decreases with increase in the magnetic field. As the baryon density is increased from vacuum to $\rho_B = \frac{\rho_0}{2}$ and subsequently to $\rho_B = \rho_0$, the Σ^{*-} baryon exhibits the same overall trend as observed for other Σ^* baryons.

In Figs. 10(a)–10(d), we plot the modification of magnetic moment of Ξ^* baryons with magnetic field. From Fig. 10(a), we can observe that the sea quark contribution of Ξ^{*0} baryon is negative, whereas all other magnetic moment contributions are positive; hence, the overall total magnetic

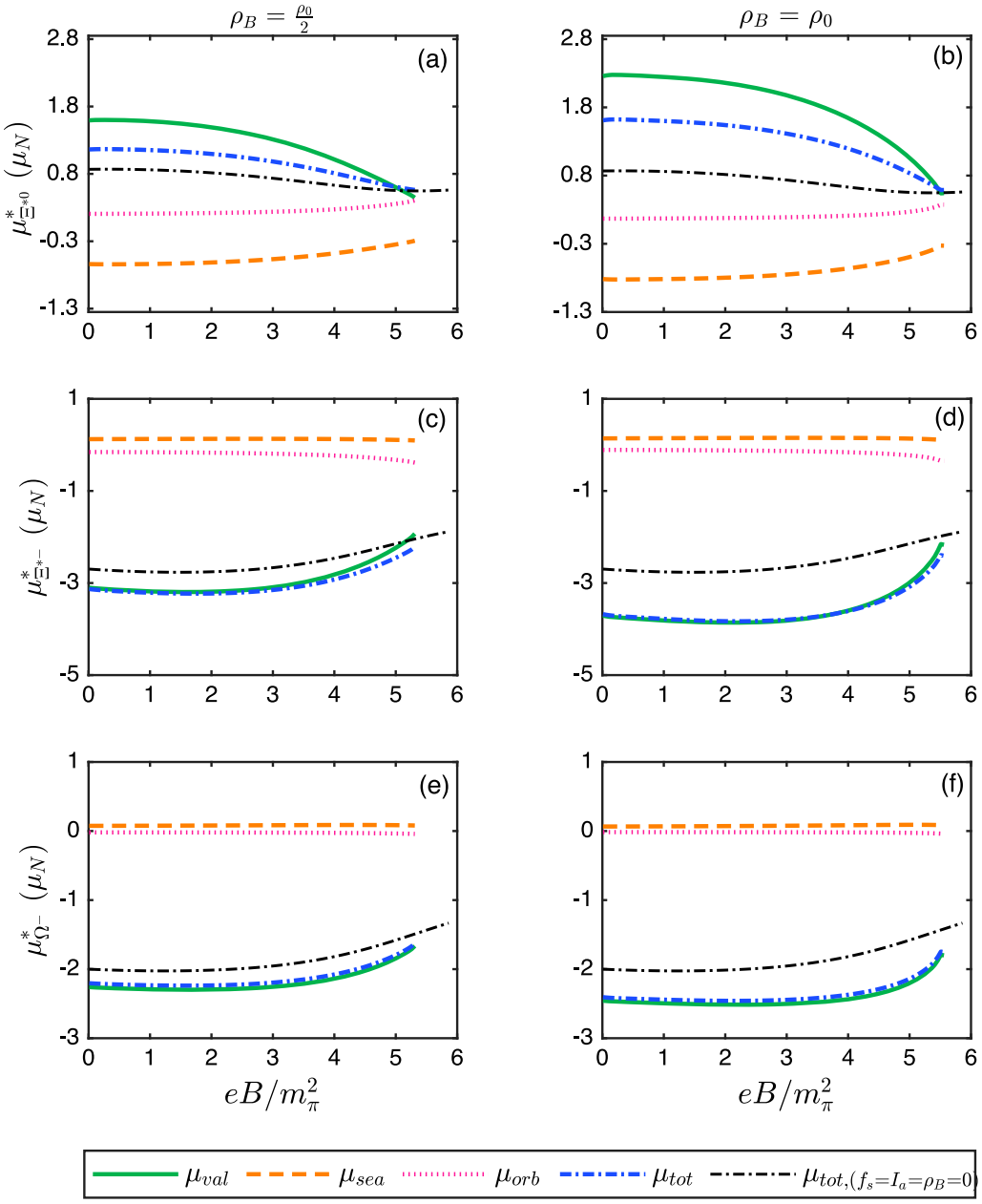


FIG. 10. In-medium magnetic moment variation of Ξ^* and Ω^- baryons as a function of magnetic field eB/m_π^2 for density $\rho_B = \frac{\rho_0}{2}$ [panels (a), (c), (e)] and $\rho_B = \rho_0$ [panels (b), (d), (f)] at $f_s = 0.7$, $I_a = 0.3$ and $T = 100$ MeV. The black dash-dotted curve corresponds to the total magnetic moment calculated for $\rho_B = 0$, $f_s = 0$, and $I_a = 0$. The different contributions to magnetic moments are shown separately in each panel.

moment remains positive. Similar to the neutral Σ^{*0} baryon shown in Figs. 9(c) and 9(d), the total magnetic moment of the Ξ^{*0} baryon, depicted in Figs. 10(a) and 10(b), decreases with increasing magnetic field. As we increase density from $\rho_B = \frac{\rho_0}{2}$ to ρ_0, the total magnetic moment of Ξ^{*0} baryon increases as discussed for Δ and Σ^* baryons. For Ξ^{*-} baryons, as shown in Figs. 10(c) and 10(d), the single d quark and two s quark contribute a negative valence moment. Therefore, the total magnetic moment remains negative at both baryon densities, and its magnitude increases gradually with increasing magnetic field up to a $eB = 1.75m_\pi^2$, beyond which it decreases. The magnetic moment due to the valence quarks and total magnetic moment differs only by 0.030 μ_N at zero magnetic field and density $\rho_B = \frac{\rho_0}{2}$ since both the sea and orbital contributions are comparatively small.

From Figs. 10(e) and 10(f), we observe that sea and orbital contributions are very small, and the magnitude of total magnetic moment of Ω^- baryon increases negligibly by a value $0.035\mu_N$ from zero magnetic field to

TABLE V. Magnetic moments of decuplet baryons at $\rho_B = 0$, $\rho_B = \frac{\rho_0}{2}$, and $\rho_B = \rho_0$ for zero magnetic field. The finite density results correspond to $f_s = 0.7$ and $I_a = 0.3$, whereas $\rho_B = 0$ corresponds to $f_s = I_a = 0$.

	Expt. values [78,110]	$\rho_B = 0$	$\rho_B = \frac{\rho_0}{2}$				$\rho_B = \rho_0$			
(μ_N)	μ_B (Free space)	μ_B^*	$\mu_{\rm val}^*$	$\mu_{\rm sea}^*$	$\mu_{\rm orb}^*$	μ_B^*	$\mu_{\rm val}^*$	$\mu_{\rm sea}^*$	$\mu_{\rm orb}^*$	μ_B^*
$\mu_{\Delta^{++}}^*$	4.5–7.5	6.464	9.468	−1.969	0.511	8.011	12.284	−2.557	0.389	10.116
$\mu_{\Delta^{+}}^*$	⋯	2.951	4.726	−1.238	0.198	3.686	6.118	−1.607	0.160	4.672
$\mu_{\Delta^{0}}^*$	⋯	−0.558	−0.018	−0.508	−0.115	−0.641	−0.062	−0.657	−0.068	−0.787
$\mu_{\Delta^{-}}^*$	⋯	−4.068	−4.768	0.224	−0.427	−4.971	−6.256	0.298	−0.297	−6.254
$\mu_{\Sigma^{*+}}^*$	⋯	3.637	5.486	−1.277	0.334	4.543	7.203	−1.658	0.254	5.799
$\mu_{\Sigma^{*-}}^*$	⋯	−3.375	−3.938	0.175	−0.291	−4.055	−4.998	0.220	−0.203	−4.981
$\mu_{\Sigma^{*0}}^*$	⋯	0.131	0.777	−0.552	0.021	0.247	1.113	−0.720	0.026	0.418
$\mu_{\Xi^{*0}}^*$	⋯	0.818	1.544	−0.589	0.157	1.113	2.208	−0.767	0.119	1.560
$\mu_{\Xi^{*-}}^*$	⋯	−2.697	−3.101	0.125	−0.155	−3.131	−3.708	0.141	−0.109	−3.676
$\mu_{\Omega^{-}}^*$	-2.02 ± 0.05	−2.000	−2.259	0.075	−0.020	−2.204	−2.456	0.066	−0.016	−2.406

TABLE VI. Same as Table V for magnetic field $eB = 3m_\pi^2$.

	$\rho_B = 0$	$\rho_B = \frac{\rho_0}{2}$				$\rho_B = \rho_0$			
(μ_N)	μ_B^*	$\mu_{\rm val}^*$	$\mu_{\rm sea}^*$	$\mu_{\rm orb}^*$	μ_B^*	$\mu_{\rm val}^*$	$\mu_{\rm sea}^*$	$\mu_{\rm orb}^*$	μ_B^*
$\mu_{\Delta^{++}}^*$	7.311	11.302	−2.343	0.609	9.568	15.864	−3.295	0.453	13.022
$\mu_{\Delta^{+}}^*$	2.801	4.546	−1.186	0.230	3.591	6.198	−1.623	0.181	4.756
$\mu_{\Delta^{0}}^*$	−0.542	−0.022	−0.436	−0.148	−0.606	−0.059	−0.590	−0.092	−0.740
$\mu_{\Delta^{-}}^*$	−4.225	−5.038	0.245	−0.527	−5.321	−7.024	0.341	−0.364	−7.046
$\mu_{\Sigma^{*+}}^*$	3.618	5.552	−1.299	0.398	4.651	7.723	−1.785	0.296	6.234
$\mu_{\Sigma^{*-}}^*$	−3.420	−4.033	0.186	−0.359	−4.206	−5.368	0.243	−0.248	−5.373
$\mu_{\Sigma^{*0}}^*$	0.064	0.597	−0.459	0.020	0.158	0.916	−0.625	0.024	0.315
$\mu_{\Xi^{*0}}^*$	0.684	1.259	−0.515	0.188	0.932	1.924	−0.700	0.139	1.363
$\mu_{\Xi^{*-}}^*$	−2.665	−3.091	0.132	−0.191	−3.149	−3.815	0.153	−0.133	−3.795
$\mu_{\Omega^{-}}^*$	−1.953	−2.256	0.084	−0.023	−2.194	−2.503	0.077	−0.018	−2.444

TABLE VII. Same as Table V for magnetic field $eB = 5m_\pi^2$.

	$\rho_B = 0$	$\rho_B = \frac{\rho_0}{2}$				$\rho_B = \rho_0$			
(μ_N)	μ_B^*	$\mu_{\rm val}^*$	$\mu_{\rm sea}^*$	$\mu_{\rm orb}^*$	μ_B^*	$\mu_{\rm val}^*$	$\mu_{\rm sea}^*$	$\mu_{\rm orb}^*$	μ_B^*
$\mu_{\Delta^{++}}^*$	5.721	7.689	−1.581	0.991	7.099	12.540	−2.587	0.716	10.669
$\mu_{\Delta^{+}}^*$	2.010	2.760	−0.711	0.357	2.407	4.168	−1.080	0.266	3.355
$\mu_{\Delta^{0}}^*$	−0.545	−0.017	−0.245	−0.276	−0.539	−0.040	−0.365	−0.183	−0.588
$\mu_{\Delta^{-}}^*$	−3.416	−3.212	0.168	−0.910	−3.954	−5.030	0.259	−0.633	−5.404
$\mu_{\Sigma^{*+}}^*$	2.727	3.387	−0.807	0.649	3.229	5.293	−1.242	0.469	4.519
$\mu_{\Sigma^{*-}}^*$	−2.748	−2.683	0.136	−0.618	−3.165	−3.942	0.194	−0.431	−4.179
$\mu_{\Sigma^{*0}}^*$	−0.024	0.241	−0.253	0.015	0.002	0.446	−0.379	0.019	0.087
$\mu_{\Xi^{*0}}^*$	0.504	0.545	−0.296	0.306	0.556	1.001	−0.442	0.221	0.781
$\mu_{\Xi^{*-}}^*$	−2.143	−2.228	0.109	−0.327	−2.446	−2.981	0.137	−0.229	−3.072
$\mu_{\Omega^{-}}^*$	−1.577	−1.841	0.085	−0.036	−1.792	−2.198	0.090	−0.026	−2.135

$eB = 1.55m_\pi^2$. Beyond that, the magnitude of the total magnetic moment of the Ω^- baryon decreases with the magnetic field as shown in Fig. 10(e). In Fig. 10(f), the total magnetic moment of the Ω^- baryon remains negative, while its magnitude increases as the baryon density is increased from vacuum to $\rho_B = \rho_0$.

Using the QMC model [51], the in-medium magnetic moments of octet, decuplet, and low-lying charm and bottom

baryons have been investigated, with a general enhancement relative to their free-space values at zero magnetic field. Calculations within χPT and LQCD yield Δ^{++} magnetic moments of $5.390\mu_N$ [52,53] and $5.240\mu_N$ [48], respectively. Furthermore, the influence of medium-modified baryonic magnetic moments on neutron-star properties under strong magnetic fields has been examined in Ref. [63], where the AMM of baryons was found to significantly modify the equation of state at high densities. In the present work, we therefore investigated the magnetic field dependence of the magnetic moments of decuplet baryons in magnetized strange matter, incorporating the effects of Landau quantization, anomalous magnetic moments, and Dirac sea contributions.

V. SUMMARY

To summarize, we investigated the in-medium effective masses and magnetic moments of the decuplet baryon in magnetized strange matter at finite temperature incorporating Dirac sea contributions, Landau quantization, and anomalous magnetic moments (AMM) using the chiral quark mean field model. We observed that the magnitudes of the scalar condensates increase with increasing magnetic field strength due to the contribution from the Dirac sea, thereby exhibiting the phenomenon of magnetic catalysis. Increasing the baryon density from $\rho_B = 0$ to ρ_0 leads to a systematic reduction in the effective masses of all decuplet baryons, reflecting the enhanced medium modification of the scalar fields. The magnetic field dependence is strongly charge and spin dependent. The charged baryons generally exhibit an initial decrease in mass followed by an increase at higher magnetic fields, resulting from the effects of AMM and Landau level contributions at low fields and magnetic catalysis at stronger fields. In contrast, neutral baryons, which do not undergo Landau quantization, show a comparatively weaker and predominantly increasing magnetic field dependence, with their spin states splitting through the AMM interaction. The magnetic moments of the decuplet baryons are evaluated using the in-medium quark and baryon masses as inputs to the chiral constituent quark model. The total magnetic moments receive contributions from valence quarks, sea quarks, and orbital angular momentum of the quark sea, with the valence contribution dominating in all cases and shows an increase in magnitude with density. The isospin asymmetry (I_a) effects are most pronounced for baryons composed of entirely of light quarks through δ meson field which induces the charge splitting within each multiplet, whereas the number of strange quarks determines the effects of strangeness fraction f_s in baryons. Therefore, Δ baryons show significant change with I_a, whereas Ω^- baryon shows more pronounced change with f_s. These results may serve as important theoretical inputs for future investigations of strongly magnetized dense matter, including magnetar interiors and the postmerger phase of binary neutron star collisions, where high density, strong magnetic fields, and strangeness coexist simultaneously. This study is also motivated by heavy-ion collision experiments at RHIC and the LHC, where extremely strong transient magnetic fields and hot dense matter are produced [1–5].

ACKNOWLEDGMENTS

H. D. would like to thank the Science and Engineering Research Board, Anusandhan-National Research Foundation (ANRF), Government of India under the SERB-POWER Fellowship scheme (Ref No. SPF/2023/000116). A. K. sincerely acknowledge Anusandhan-National Research Foundation (ANRF), Government of India, for funding of the research project under the Science and Engineering Research Board-Core Research Grant (SERB-CRG) scheme (File No. CRG/2023/000557) for financial support.

DATA AVAILABILITY

There are no publicly available research data or software supporting this paper. Requests for further information or data should be sent to the authors.

[1] D. E. Kharzeev, L. D. McLerran, and H. J. Warringa, Nucl. Phys. **A803**, 227 (2008).
[2] V. Skokov, A. Illarionov, and V. Toneev, Int. J. Mod. Phys. A **24**, 5925 (2009).
[3] V. Voronyuk, V. D. Toneev, W. Cassing, E. L. Bratkovskaya, V. P. Konchakovski, and S. A. Voloshin, Phys. Rev. C **83**, 054911 (2011).
[4] A. Bzdak and V. Skokov, Phys. Lett. B **710**, 171 (2012).
[5] W.-T. Deng and X.-G. Huang, Phys. Rev. C **85**, 044907 (2012).
[6] J. Bloczynski, X.-G. Huang, X. Zhang, and J. Liao, Phys. Lett. B **718**, 1529 (2013).
[7] L. McLerran and V. Skokov, Nucl. Phys. **A929**, 184 (2014).
[8] K. Tuchin, Phys. Rev. C **93**, 014905 (2016).
[9] Y. Chen, X.-L. Sheng, and G.-L. Ma, Nucl. Phys. **A1011**, 122199 (2021).
[10] K. Fukushima, D. E. Kharzeev, and H. J. Warringa, Phys. Rev. D **78**, 074033 (2008).
[11] G. S. Bali, F. Bruckmann, G. Endrodi, F. Gruber, and A. Schafer, J. High Energy Phys. 04 (2013) 130.

[12] D. E. Kharzeev and D. T. Son, Phys. Rev. Lett. **106**, 062301 (2011).
[13] D. E. Kharzeev, J. Liao, S. A. Voloshin, and G. Wang, Prog. Part. Nucl. Phys. **88**, 1 (2016).
[14] D. E. Kharzeev and J. Liao, Nat. Rev. Phys. **3**, 55 (2021).
[15] X.-G. Huang, Rep. Prog. Phys. **79**, 076302 (2016).
[16] V. P. Gusynin, V. A. Miransky, and I. A. Shovkovy, Nucl. Phys. **B462**, 249 (1996).
[17] V. A. Miransky and I. A. Shovkovy, Phys. Rev. D **66**, 045006 (2002).
[18] G. S. Bali, F. Bruckmann, G. Endrődi, Z. Fodor, S. D. Katz, and A. Schäfer, Phys. Rev. D **86**, 071502 (2012).
[19] W. Li and G. Wang, Annu. Rev. Nucl. Part. Sci. **70**, 293 (2020).
[20] A. Huang, D. She, S. Shi, M. Huang, and J. Liao, Phys. Rev. C **107**, 034901 (2023).
[21] K. Fukushima, Prog. Part. Nucl. Phys. **107**, 167 (2019).
[22] I. A. Shovkovy, Particles **5**, 442 (2022).
[23] H. Taya, Phys. Rev. D **92**, 014038 (2015).
[24] N. O. Agasian and S. M. Fedorov, Phys. Lett. B **663**, 445 (2008).
[25] G. S. Bali, F. Bruckmann, G. Endrődi, Z. Fodor, S. D. Katz, S. Krieg, A. Schäfer, and K. K. Szabó, J. High Energy Phys. 02 (2012) 044.
[26] Sh. Fayazbakhsh, and N. Sadooghi, Phys. Rev. D **90**, 105030 (2014).
[27] W. R. Tavares, S. S. Avancini, R. L. S. Farias, and R. P. Cardoso, Phys. Rev. D **109**, 016011 (2024).
[28] E. S. Fraga, L. F. Palhares, and C. Villavicencio, Phys. Rev. D **109**, 116018 (2024).
[29] S. Fajfer and R. J. Oakes, Phys. Rev. D **28**, 2881 (1983).
[30] G. Başar, G. V. Dunne, and D. E. Kharzeev, Phys. Rev. D **85**, 045026 (2012).
[31] P. V. Buividovich, M. N. Chernodub, E. V. Luschevskaya, and M. I. Polikarpov, Phys. Rev. D **81**, 036007 (2010).
[32] A. E. Broderick, M. Prakash, and J. M. Lattimer, Phys. Lett. B **531**, 167 (2002).
[33] M. Sinha, B. Mukhopadhyay, and A. Sedrakian, Nucl. Phys. **A898**, 43 (2013).
[34] A. Rabhi, P. K. Panda, and C. Providencia, Phys. Rev. C **84**, 035803 (2011).
[35] D. P. Menezes, M. B. Pinto, S. S. Avancini, A. Pérez Martínez, and C. Providência, Phys. Rev. C **79**, 035807 (2009).
[36] J. Moreira, P. Costa, and T. E. Restrepo, Eur. Phys. J. A **57**, 123 (2021).
[37] Y. Wang and X.-J. Wen, Phys. Rev. D **105**, 074034 (2022).
[38] P. Yue and H. Shen, Phys. Rev. C **77**, 045804 (2008).
[39] V. Dexheimer, R. Negreiros, and S. Schramm, Eur. Phys. J. A **48**, 189 (2012).
[40] N. Chahal, S. Dutt, and A. Kumar, Phys. Rev. C **107**, 045203 (2023).
[41] P. C. Chu, X.-H. Li, H.-Y. Ma, B. Wang, Y.-M. Dong, and X.-M. Zhang, Phys. Lett. B **778**, 447 (2018).
[42] D. P. Menezes, M. B. Pinto, S. S. Avancini, and C. Providência, Phys. Rev. C **80**, 065805 (2009).
[43] A. Haber, F. Preis, and A. Schmitt, Phys. Rev. D **90**, 125036 (2014).
[44] A. Mukherjee, S. Ghosh, M. Mandal, S. Ghosh, M. Mandal, S. Sarkar, and P. Roy, Phys. Rev. D **98**, 056024 (2018).
[45] R. M. Aguirre and A. L. De Paoli, Eur. Phys. J. A **52**, 343 (2016).
[46] R. M. Aguirre, Phys. Rev. C **100**, 065203 (2019).
[47] M. J. Savage, Nucl. Phys. **A700**, 359 (2002).
[48] D. B. Leinweber, T. Draper, and R. M. Woloshyn, Phys. Rev. D **46**, 3067 (1992).
[49] C. Alexandrou, T. Korzec, G. Koutsou, and T. Leontiou, Phys. Rev. D **79**, 014507 (2009).
[50] K. Tsushima, K. Saito, J. Haidenbauer, and A. W. Thomas, Nucl. Phys. **A630**, 691 (1998).
[51] K. Tsushima, Prog. Theor. Exp. Phys. **2022**, 043D02 (2022).
[52] L. S. Geng, J. M. Camalich, and M. J. V. Vacas, Phys. Rev. D **80**, 034027 (2009).
[53] R. Flores Mendieta, Phys. Rev. D **80**, 094014 (2009).
[54] F. X. Lee, R. Kelly, L. Zhou, and W. Wilcox, Phys. Lett. B **627**, 71 (2005).
[55] H. Singh, A. Kumar, and H. Dahiya, Chin. Phys. C **41**, 094104 (2017).
[56] H. Singh, A. Kumar, and H. Dahiya, Eur. Phys. J. Plus **134**, 128 (2019).
[57] H. Singh, A. Kumar, and H. Dahiya, Eur. Phys. J. A **54**, 120 (2018).
[58] H. Singh, A. Kumar, and H. Dahiya, Eur. Phys. J. Plus **135**, 422 (2020).
[59] N. Sharma, H. Dahiya, P. K. Chatley, and M. Gupta, Phys. Rev. D **81**, 073001 (2010).
[60] A. Girdhar, H. Dahiya, and M. Randhawa, Phys. Rev. D **92**, 033012 (2015).
[61] A. Kaur and A. Upadhyay, Eur. Phys. J. A **52**, 105 (2016).
[62] Z. Rezaei, Int. J. Mod. Phys. E **27**, 1850011 (2018).
[63] C. Y. Ryu and K. S. Kim, Phys. Rev. C **82**, 025804 (2010).
[64] D. Fu, B.-D. Sun, and Y. Dong, Phys. Rev. D **105**, 096002 (2022).
[65] L.-Z. Wen, Y.-K. Chen, L. Meng, and S.-L. Zhu, Eur. Phys. J. C **85**, 1210 (2025).
[66] A. Manohar and H. Georgi, Nucl. Phys. **B234**, 189 (1984).
[67] T. P. Cheng and L.-F. Li, Phys. Rev. Lett. **80**, 2789 (1998).
[68] V. Bernard, N. Kaiser, and U.-G. Meissner, Int. J. Mod. Phys. E **04**, 193 (1995).
[69] R. K. Sahoo, A. R. Panda, and A. Nath, Phys. Rev. D **52**, 4099 (1995).
[70] A. J. Buchmann and E. M. Henley, Phys. Rev. D **65**, 073017 (2002).
[71] T. Ledwig, A. Silva, and M. Vanderhaeghen, Phys. Rev. D **79**, 094025 (2009).
[72] A. Bosshard *et al.*, Phys. Rev. D **44**, 1962 (1991).
[73] H. T. Diehl *et al.*, Phys. Rev. Lett. **67**, 804 (1991).
[74] N. B. Wallace, P. M. Border, D. P. Ciampa, G. Guglielmo, K. J. Heller, D. M. Woods, K. A. Johns, Y. T. Gao, M. J. Longo, and R. Rameika, Phys. Rev. Lett. **74**, 3732 (1995).
[75] M. Kotulla *et al.*, Phys. Rev. Lett. **89**, 272001 (2002).
[76] F. Schlumpf, Phys. Rev. D **48**, 4478 (1993).
[77] F. X. Lee, Phys. Rev. D **57**, 1801 (1998).
[78] J. Linde, T. Ohlsson, and H. Snellman, Phys. Rev. D **57**, 452 (1998).
[79] H. Dahiya and M. Gupta, Phys. Rev. D **67**, 114015 (2003).
[80] H. Dahiya, J. Phys. Soc. Jpn. Conf. Proc. **26**, 021019 (2019).
[81] A. Kumar, S. Dutt, and H. Dahiya, Eur. Phys. J. A **60**, 4 (2024).

[82] U. Dastidar, A. Kumar, H. Dahiya, and S. Dutt, Prog. Theor. Exp. Phys. **2026**, ptag155 (2026).
[83] P. Wang, Z. Y. Zhang, Y. W. Yu, R. K. Su, and Q. Song, Nucl. Phys. **A688**, 791 (2001).
[84] P. Papazoglou *et al.*, Phys. Rev. C **59**, 411 (1999).
[85] A. Mishra, A. Kumar, and S. P. Misra, Phys. Rev. D **110**, 014003 (2024).
[86] W. Ping, Z. Zong-Ye, and Y. You-Wen, Commun. Theor. Phys. **36**, 71 (2001).
[87] A. Broderick, M. Prakash, and J. M. Lattimer, Astrophys. J. **537**, 351 (2000).
[88] F. X. Wei, G. J. Mao, C. M. Ko, L. S. Kisslinger, H. Stöcker, and W. Greiner, J. Phys. G **32**, 47 (2006).
[89] G.-J. Mao, A. Iwamoto, and Z.-X. Li, Chin. J. Astron. Astrophys. **3**, 359 (2003).
[90] L. D. Landau and D. ter Haar, *Collected Papers of L. D. Landau* (Pergamon Press, New York, 1965).
[91] N. Barik, A. Mishra, and B. K. Dash, Phys. Rev. C **88**, 015206 (2013).
[92] N. Barik, B. K. Dash, and M. Das, Phys. Rev. D **31**, 1652 (1985).
[93] M. Kumari and A. Kumar, Eur. Phys. J. Plus **136**, 19 (2021).
[94] R. Kumar and A. Kumar, Chin. Phys. C **43**, 124109 (2019).
[95] R. Kumar and A. Kumar, Eur. Phys. J. C **79**, 403 (2019).
[96] D. H. Constantinescu, Nucl. Phys. **B36**, 121 (1972).
[97] P. Parui, S. De, A. Kumar, and A. Mishra, Phys. Rev. D **106**, 114033 (2022).
[98] S. De, P. Parui, and A. Mishra, Phys. Rev. C **107**, 065204 (2023).
[99] S. De, P. Parui, and A. Mishra, Int. J. Mod. Phys. E **31**, 2250106 (2022).
[100] P. Wang, V. E. Lyubovitskij, T. Gutsche, and A. Faessler, Phys. Rev. C **67**, 015210 (2003).
[101] K. D. Marquez, M. R. Pelicer, S. Ghosh, J. Peterson, D. Chatterjee, V. Dexheimer, and D. P. Menezes, Phys. Rev. C **106**, 035801 (2022).
[102] T. P. Cheng and L. F. Li, Phys. Rev. Lett. **74**, 2872 (1995).
[103] T. P. Cheng and L. F. Li, Phys. Rev. D **57**, 344 (1998).
[104] X. Song, J. S. McCarthy, and H. J. Weber, Phys. Rev. D **55**, 2624 (1997).
[105] X. Song, Phys. Rev. D **57**, 4114 (1998).
[106] H. Dahiya and M. Gupta, Phys. Rev. D **64**, 014013 (2001).
[107] H. Dahiya and M. Gupta, Int. J. Mod. Phys. A **19**, 5027 (2004).
[108] H. Dahiya, M. Gupta, and J. M. S. Rana, Int. J. Mod. Phys. A **21**, 4255 (2006).
[109] H. Dahiya, S. Dutt, A. Kumar, and M. Randhawa, Eur. Phys. J. Plus **138**, 441 (2023).
[110] K. Hagiwara *et al.*, Phys. Rev. D **66**, 010001 (2002).